Crustal structure of the rifted volcanic margins and uplifted plateau of Western Yemen from receiver function analysis

Abdulhakim Ahmed,[1,2,3] Christel Tiberi,[4] Sylvie Leroy,[2,3] Graham W. Stuart,[5] Derek Keir,[6] Jamal Sholan,[1] Khaled Khanbari,[7] Ismael Al-Ganad[8] and Clémence Basuyau[9]

[1] *Seismological and Volcanological Observatory Center, Dhamar, Yemen. E-mail: hakim66@myself.com*
[2] *Univ. Paris 06 CNRS ISTEP-UPMC, Paris, France*
[3] *CNRS UMR7193, iSTEP, Paris, France*
[4] *CNRS Géosciences Montpellier, France*
[5] *School of Earth and Environment, University of Leeds, Leeds, UK*
[6] *National Oceanography Centre Southampton, University of Southampton, Southampton, UK*
[7] *Yemen Remote Sensing Center and Department of Earth and Environmental Science, Sana'a University Yemen, Yemen*
[8] *Yemen Geological Survey & Mineral Resources Board, Sana'a, Yemen*
[9] *Institut de Physique du Globe de Paris, Paris, France*

SUMMARY

We analyse *P*-wave receiver functions across the western Gulf of Aden and southern Red Sea continental margins in Western Yemen to constrain crustal thickness, internal crustal structure and the bulk seismic velocity characteristics in order to address the role of magmatism, faulting and mechanical crustal thinning during continental breakup. We analyse teleseismic data from 21 stations forming the temporary Young Conjugate Margins Laboratory (YOCMAL) network together with GFZ and Yemeni permanent stations. Analysis of computed receiver functions shows that (1) the thickness of unextended crust on the Yemen plateau is ∼35 km; (2) this thins to ∼22 km in coastal areas and reaches less than 14 km on the Red Sea coast, where presence of a high-velocity lower crust is evident. The average Vp/Vs ratio for the western Yemen Plateau is 1.79, increasing to ∼1.92 near the Red Sea coast and decreasing to 1.68 for those stations located on or near the granitic rocks.

Thinning of the crust, and by inference extension, occurs over a ∼130-km-wide transition zone from the Red Sea and Gulf of Aden coasts to the edges of the Yemen plateau. Thinning of continental crust is particularly localized in a <30-km-wide zone near the coastline, spatially co-incident with addition of magmatic underplate to the lower crust, above which on the surface we observe the presence of seaward dipping reflectors (SDRs) and thickened Oligo-Miocene syn-rift basaltic flows. Our results strongly suggest the presence of high-velocity mafic intrusions in the lower crust, which are likely either synrift magmatic intrusion into continental lower crust or alternatively depleted upper mantle underplated to the base of the crust during the eruption of the SDRs. Our results also point towards a regional breakup history in which the onset of rifting was synchronous along the western Gulf of Aden and southern Red Sea volcanic margins followed by a second phase of extension along the Red Sea margin.

Key words: Broad-band seismometers; Continental margins: divergent; Large igneous provinces; Kinematics of crustal and mantle deformation; Africa.

INTRODUCTION

During the breakup of continents, the lithosphere deforms by faulting, ductile stretching and thinning (McKenzie 1978), and in volcanic rifts also by magma (Ebinger & Casey 2001; Buck *et al.* 2006). Despite the importance of breakup in plate tectonics, we have few constraints on the spatial and temporal relationship between plate stretching and magma intrusion, and how these processes relate to the eruption of voluminous basalt flows that characterize magmatic margins worldwide (e.g. White *et al.* 2008). We address this problem by imaging crustal structure (thickness and average seismic properties) using *P*-wave receiver functions (Burdick & Langston 1977; Langston 1977; Ammon 1991) at the young (∼30 Ma) Red Sea and Gulf of Aden rifted volcanic margins in the SW corner

GJI Seismology

of Arabia, where the margin preserves the rift morphology resultant from breakup, and where the syn-rift geology and stratigraphic record has not yet been completely obscured by thick post-rift sediments (Davison *et al.* 1994). Furthermore, the margin captures the change from magma-rich breakup in Western Yemen to magma-poor breakup in the eastern Gulf of Aden (Leroy *et al.* 2010b), thus establishing a framework from which to interpret controls on the along-rift variability in melt supply.

Crustal thickness variations and the identification of magmatic input into the crust are key parameters in quantifying the locus and amount of tectonic stretching and associated thinning, as well as magmatic addition during continental rifting. We used 21 broad-band seismic stations, the majority deployed for ~1 yr (March 2009–February 2010) as a part of the Young Conjugate Margins Laboratory (YOCMAL) in Yemen. These stations are mainly from

two profiles in Yemen that run perpendicular to the major tectonic features in western Gulf of Aden, and southern Red Sea. We also use data from a collection of stations distributed near to the Red Sea coast to capture lateral variations in crustal thickness and internal properties along the rift margin near the SW tip of Arabia (Fig. 1). We particularly focus on the relationship between magmatic intrusion, mechanical crustal thinning and the volcanic geology formed during the opening of these two rifts.

TECTONIC SETTING

The rifted margins of Yemen are located at the south-western corner of the Arabian Peninsula (Fig. 1), bounded to the west by the Red Sea and to the south by the Gulf of Aden. These two Oligocene spreading centres separate Arabia from the Nubia and Somalia plates,
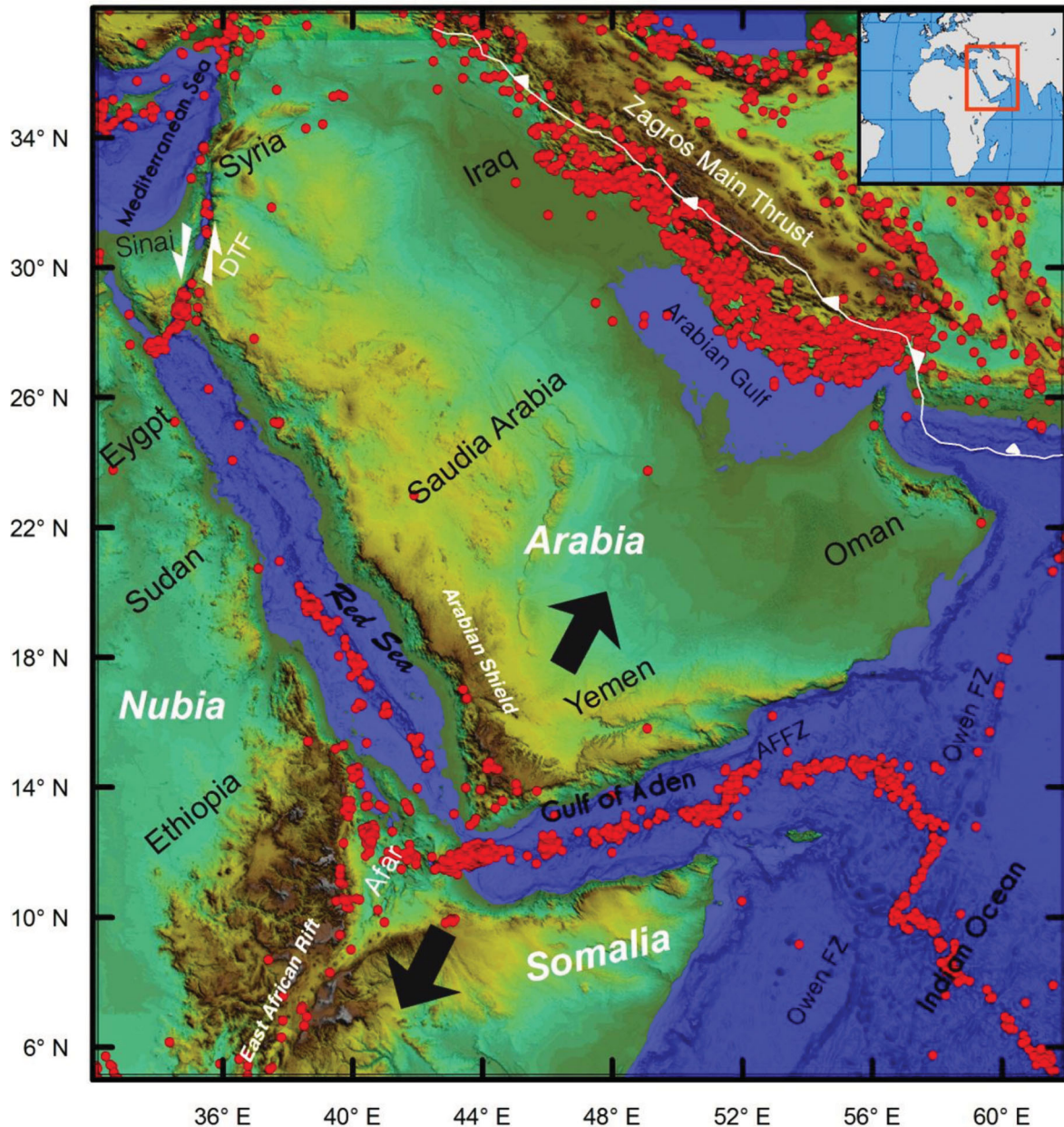
Figure 1. Land-sat imagery and Sea-sat bathymetry showing the seismicity along the boundaries between Arabian plate and adjacent areas. The seismic data are extracted from ISC seismic catalogue for the period January 1970–February 2012 and $M \geq 5.0$ (International Seismological Centre 2012). AFFZ is Alula-Fartaq fracture zone. The large black arrows are pointing to the direction of motion of different plates in the region.
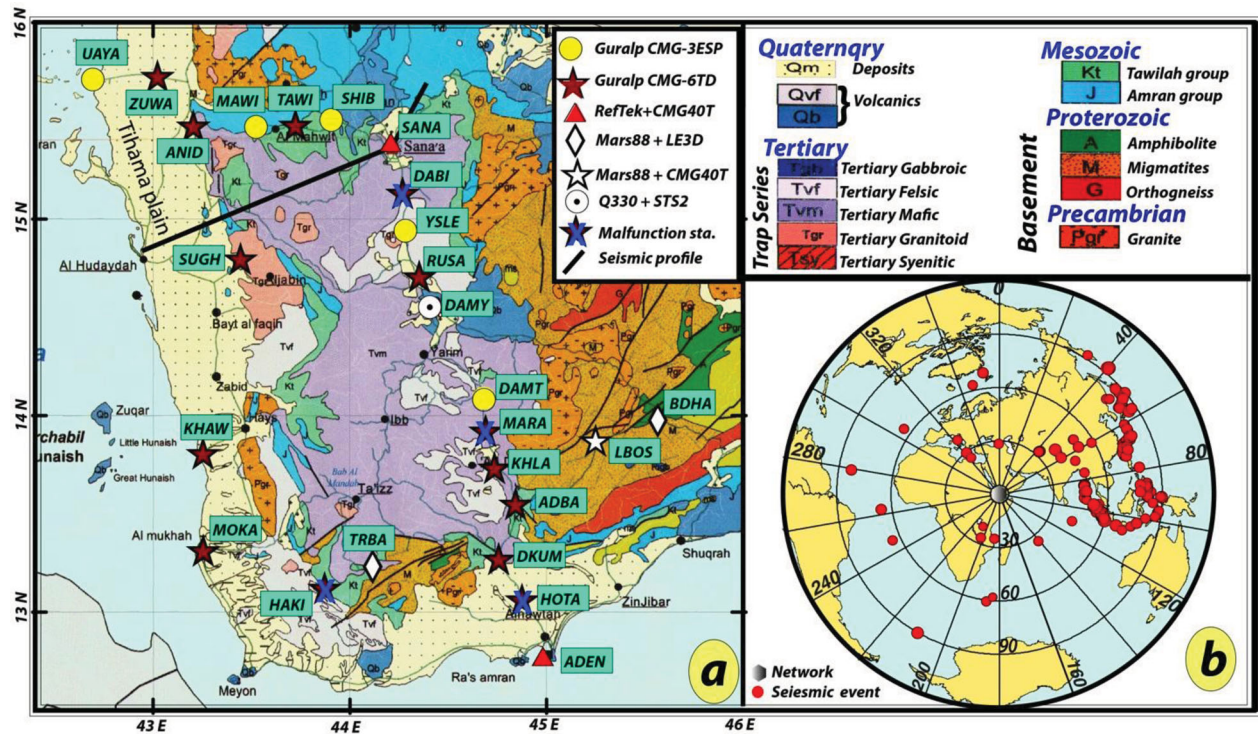
Figure 2. (a) Geological map of the study area showing different geological units (modified from Geological Survey and Mineral Resources Board—Yemen), with the seismic stations location for the western area of YOCMAL project and stations from Yemen permanent seismic network. The thick black line shows the location of the SONNE 1988 seismic profile. (b) Backazimuth events distribution of the events on a projection centred on the North Pole. Circles are every 10° of distance.

with the East African rift forming the third arm at the Afar triple junction (Fig. 1) (McKenzie *et al.* 1970). Red Sea and Gulf of Aden rifting started in Oligocene times 30 Ma ago, coeval with a peak in eruption of the voluminous Ethiopia–Yemen flood basalt province (e.g. Courtillot *et al.* 1999; Ukstins *et al.* 2002; Wolfenden *et al.* 2005). In the Gulf of Aden, the mean extension of N25°E is oblique to the N75°E strike of the rift, and the rate of extension increases from west (1.6 cm yr^{-1}) to east (2.3 cm yr^{-1}) (Jestin *et al.* 1994; Fournier *et al.* 2001; Leroy *et al.* 2004; Fournier *et al.* 2010). The Red Sea has an extension rate that ranges from ∼0.9 cm yr^{-1} in the north to ∼1.5 cm yr^{-1} in the south (e.g. Jestin *et al.* 1994; Chu & Gordon 1998; Demets *et al.* 2010). The opening kinematics in the southern Red Sea is more complex since the locus of strain likely shifted westward onland into Afar at ∼11 Ma (e.g. Chu & Gordon 1998; Eagles *et al.* 2002).

The presence of the Afar plume to the south has been used by Leroy *et al.* (2010b) to explain the change from a magmatic margin in the west of the Gulf of Aden to a magma-poor margin in the east. Asthenospheric flow from the Afar plume has been proposed to explain the magmatic characteristics of breakup in the Gulf of Aden as well as the anomalously low seismic velocities in the upper mantle beneath the shoulders of both the Gulf of Aden and Red Sea rifts (e.g. Hansen *et al.* 2007; Leroy *et al.* 2010a; Chang & Van der Lee 2011; Chang *et al.* 2011). Although the eastern Gulf of Aden margin, off-shore Oman, is described as magmatically poor, the presence of mafic underplate at the base of the crust suggests limited post-rift magmatism did indeed occur after breakup (Lucazeau *et al.* 2009; Autin *et al.* 2010; d'Acremont *et al.* 2010; Watremez *et al.* 2011). In addition to the presence of an upper mantle low-velocity anomaly, which currently imaged below the margin (Basuyau *et al.* 2010). In the Red Sea, pervasive magma intrusion in the form of dike swarms and granite plutonism as well as the presence of evaporite deposits

in the upper crust (Mohr 1991; Davison *et al.* 1994) changes crustal rheology and likely influences where and how strain localizes.

In southwestern Yemen the Proterozoic basement is unconformably overlain by Permian Akbra shale, lower Jurassic Kohlan sandstone, upper Jurassic Amran limestone and Cretaceous continental Tawilah sandstones (Davison *et al.* 1994; Beydoun 1997). In the Tertiary, the flood basalt volcanic trap series erupted and covered most of the study area to thicknesses of up to 3 km (Fig. 2). On the ∼40-km-wide Red Sea Tihama coastal plain, the structural basement is overlaid by Miocene to recent clastics and evaporates up to ∼4000 m thick (El-Anbaawy *et al.* 1992; Davison *et al.* 1994) (Fig. 2). In the Gulf of Aden coastal plain, near Aden city syn-rift volcanic seaward dipping reflectors (SDRs) are seen overlying the basement (Tard *et al.* 1991; Leroy *et al.* 2012).

DATA AND METHODOLOGY

During the seismological part of the YOCMAL project (e.g. Leroy *et al.* 2010c), ∼50 broadband seismic stations were distributed in three areas of Yemen (West, Central and East). In this paper, we study the western area. The station distribution was designed to be perpendicular to the main axes of the two rifting systems: the Gulf of Aden and the Red Sea (Fig. 2). The seismic network was equipped with Guralp seismometers, 11 CMG-3ESP (60 s natural period) sensors, 36 CMG-6TD (30 s natural period) sensors and 4 CMG-40T (30 s natural period) sensors. The permanent GFZ station DAMY is equipped with STS-2 seismometer and Quantera-330 datalogger. Three stations of the Yemen permanent network are included (LBOS, BDHA and TRBA)—Fig. 2(a). TRBA and BDHA are equipped with Mars-88 digitizers and LE3D sensors, while LBOS is equipped with Mars-88 digitizer and CMG-40T

Table 1. Crustal thickness (*H*) and *Vp/Vs* ratio results for seismic stations of western profile—western Yemen. The average crustal velocity used is 6.2 km s^{-1} for all of the plateaue and most of the coastal plain stations, except UAYA and ZUWA(SW) where 5.3 km s^{-1} is used. The average crustal velocity is derived from Egloff *et al.* (1991).

Location	Station name	Number of RF	Latitude (N)	Longitude (E)	Elevation (m)	Crustal thickness (km)	*Vp/Vs* ratio	Error in depth (km)	Error in *Vp/Vs*	Poisson's Ratio (σ)
S to N Section	ADEN	45	12.77592	44.98244	59	20.4	1.73	2.08	0.057	0.25
	DKUM	19	13.27108	44.75736	397	23.6	1.69	0.37	0.030	0.23
	ADBA	36	13.55078	44.84239	705	31	1.68	1.78	0.053	0.23
	KHLA	21	13.79685	44.80798	1457	33.8	1.75	5.99	0.090	0.26
	DAMT	35	14.08737	44.68227	1902	35.2	1.83	0.42	0.017	0.29
	DAMY	30	14.57133	44.39000	2460	35.2	1.79	2.28	0.051	0.27
	RUSA	29	14.70738	44.35394	2332	35.2	1.76	1.49	0.035	0.26
	YSLE	43	14.93873	44.28157	2557	35.0	1.77	0.49	0.020	0.27
	SANA	34	15.39263	44.20682	2253	35.4	1.78	1.32	0.034	0.27
E to W section	SHIB	33	15.50305	43.90550	2630	35.8	1.80	2.76	0.056	0.28
	TAWI	26	15.47866	43.72389	2333	32.2	1.79	1.99	0.049	0.27
	MAWI	36	15.46748	43.52317	1875	31.4	1.74	2.98	0.064	0.25
	ANID	23	15.47365	43.20478	147	22.8	1.83	0.46	0.031	0.29
	ZUWA	27	15.72752	43.02184	87	23.0	1.91	1.95	0.057	0.31
	UAYA	28	15.70929	42.69337	9	13.8	1.92	0.26	0.027	0.31
Along Red Sea	SUGH	10	14.79705	43.44282	248	23.2	1.73	2.17	0.044	0.25
	KHAW	30	13.80802	43.25408	14	23.0	1.68	0.34	0.138	0.23
	MOKA	25	13.31374	43.25631	29	21.5	1.85	3.35	0.061	0.29
Parallel to Gulf of Aden	TRBA	77	13.231	44.116	1860	27.4	1.86	1.37	0.054	0.30
	LBOS	49	13.871	45.250	2325	32.6	1.83	0.53	0.018	0.29
	BDHA	29	13.975	45.567	2000	36.2	1.76	0.62	0.029	0.26

sensor. The temporary seismic stations were continuously recorded from March 2009 until February 2010 at 40 sps; DAMY records at both 100 and 20 sps; the Yemen network stations operated in trigger mode with a sampling rate of 62.5 sps. All stations were equipped with a GPS timing system operated in continuous mode to synchronize the stations internal clock. Maintenance and data collection were carried out every 3 months during the recording period.

In this paper, we study the western profile (Fig. 2), which can be divided into three sections: (1) A N-S section (Fig. 2a), which extends from the northern margin of Gulf of Aden up to Sana'a on the plateau, has nine stations (SANA, YSLE, RUSA, DAMY, DAMT, KHLA, ADBA, DKUM and ADEN). (2) An E-W section in the NW of Yemen, from the eastern margin of the Red Sea across the Tihama plain to Sana'a on the plateau. This has 6 stations (SHIB, MAWI, TAWI, ANID, ZUWA and UAYA). (3) A three-station section located parallel to the southern Red Sea coast consists of SUGH, KHAW and MOKA.

During the operation period of the network, >100 teleseismic earthquakes within the epicentral distance range (25°–95°) and with Mw >5.5 were recorded. Based on the signal-to-noise ratio, we selected the best waveform data recorded at each station. The number of events included in the final analysis varies from 10 to 47 per site (Table 1), depending on the background noise and the state of health of the station. Most of the selected events come from ENE of Yemen with some events from the south and from the northwest (Fig. 2b). A lack of large magnitude earthquakes from southerly backazimuths (150°–300°) results in an inhomogeneous distribution of events, and hence insufficient data for detailed analysis of crustal anisotropy using receiver functions (e.g. Frederiksen *et al.* 2003).

The waveform of teleseismic *P* waves, recorded at three-component broadband stations, is dependent on the instrument response, source radiation pattern, propagation path and local crustal structure beneath the station. By removing the effects of the source, propagation path and instrument response using the receiver function technique (e.g. Langston 1977, 1979), the information of the local crustal structure beneath the station can be derived from *P*-wave to *S*-wave conversions (Owens *et al.* 1984; Ammon 1991). In this study, we use the iterative time domain deconvolution technique, developed by Ligorria & Ammon (1999), to compute receiver functions.

We filter our raw waveforms with a zero-phase Butterworth bandpass filter with corner frequencies of 0.02–0.8 Hz. The N-S and E-W horizontal components are rotated to radial and tangential components. A 30 s time window (5 s before the theoretical *P* arrival time and 25 s after) is used to deconvolve the vertical component from the radial and transverse to calculate the receiver functions. Following Ligorria & Ammon (1999), we apply a Gaussian filter of 2.5 s to the deconvolved spike wave train, except for the noisiest stations where a Gaussian width of 2.0 is used.

Crustal thickness (*H*) and the average crustal *Vp/Vs* ratio (*k*) are initially determined using the *H-k* domain stacking technique (Zhu & Kanamori 2000). There is an inherent trade-off in receiver function analysis between crustal thickness and average crustal velocity properties (Ammon *et al.* 1990). The *H-k* stacking algorithm reduces this ambiguity by summing amplitudes of the receiver function for Moho P-to-S conversion Ps and its multiple converted phases, PpPs and PpSs+PsPs (Fig. 3e) at predicted arrival times using different crustal thickness *H* and *Vp/Vs* values.

The stacking amplitude in the *H-k* domain is then given by

$$s(H, K) = \sum_{m=1}^{n} W_1 r_m\left(t_{P_s}\right) + W_2 r_m\left(t_{P_p P_s}\right)$$

$$- W_3 r_m\left(t_{P_p S_s + P_s P_s}\right), \tag{1}$$

where *n* is the number of receiver functions, W_j is a weighting factor that represents the contribution of the corresponding seismic phase
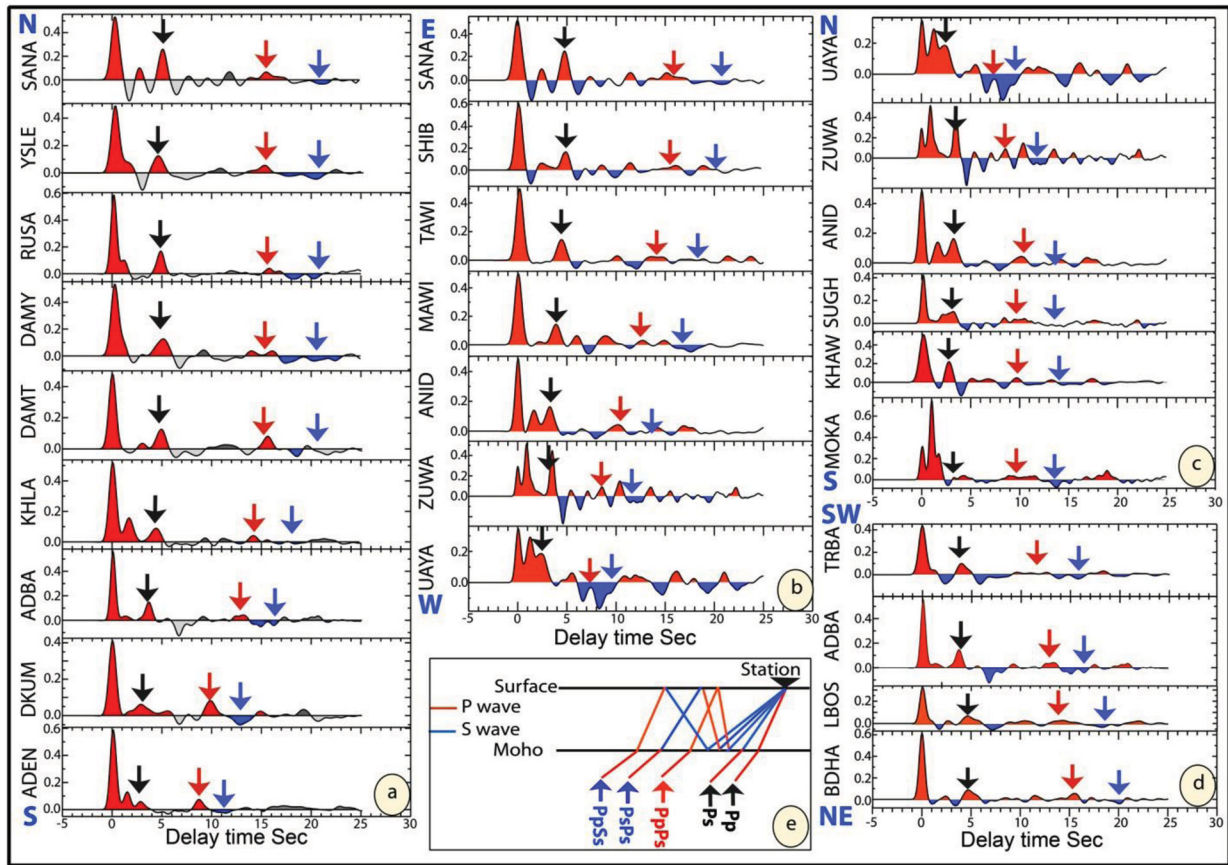
Figure 3. Stacked receiver functions for 16 seismic stations of our study: (a) for north–south section of the profile, (b) for the east–west section, (c) stations along Red Sea coast and (d) stations parallel to Gulf of Aden. The arrows represent the arrival of the Moho Ps (black), PpPs (red) and PpSs+PsPs (blue) phases from the Moho. See inset in (e) for explanation of the Moho Ps and the multiple phases crustal paths.

according to signal-to-noise ratio ($W_1 + W_2 + W_3 = 1$) and $r_m(t)$ is the amplitude of the receiver function at time t of the associated seismic phase. When the three phases stack constructively, s(H,k) reaches its maximum; this represents the best estimate for both H and Vp/Vs (k) beneath the station. The weighting factors used in this study for most of the stations are $W_1 = 0.6$, $W_2 = 0.3$ and $W_3 = 0.1$ (Zhu & Kanamori 2000). Only in few cases, when the Moho conversion phase amplitude is low or when high-amplitude intra-crustal interfaces conversion phase obscured the Moho Ps conversion, did we modify the weighting factors. We choose a value of 6.2 km s^{-1} for average crustal *P*-wave velocity (Vp), in agreement with previous controlled-source seismic work in the region (e.g. Egloff *et al.* 1991). We estimate the standard deviation for both crustal thickness H and Vp/Vs ratio with a bootstrap resampling technique (Efron & Tibshirani 1986). The bootstrap analysis was done for random subsets of data for each station, and the dispersion of the result gives the error bars mentioned in the depth sections. We applied the same technique to estimate the error coming from the average *P*-wave velocity used in the inversions (Tiberi *et al.* 2007). Another advantage of this (H,k) stacking method is that it gives an indication of average crustal composition with a local estimate of Vp/Vs value (e.g. Christensen 1996). This ratio is related to the Poisson's ratio through a simple relationship (Zandt & Ammon 1995; Ligorria 2000), and its variations depend on crustal mineralogy (felsic, mafic), the presence of fluids and physical properties of the rocks.

To refine our crustal model into upper and lower crustal layers, we invert a stack of the radial receiver functions with a stochastic method (Shibutani *et al.* 1996). We use the Neighborhood Al-

gorithm (NA) technique (Sambridge 1999a,b) to invert for a 1-D crustal shear wave velocity–depth distribution beneath a number of our sites. The initial model is based on wide-angle reflection and refraction seismic profiling results (e.g. Egloff *et al.* 1991, Fig. 2), and the Vp/Vs ratio is estimated from *H-k* stacking results. We invert for a model, which is composed of four to five layers: a sediment layer, when needed, basement, upper crust, lower crust and uppermost mantle. In each layer, the model parameters are layer thickness, shear wave velocity at the upper and lower boundaries of the layer and the layer Vp/Vs ratio. The receiver function parameterization and calculation follow the one implemented by Shibutani *et al.* (1996).

RESULTS

Our crustal model results, tabulated in Table 1, exclude the stations DABI, MARA, HOTA and HQBA (Fig. 2a), due to their malfunction, which resulted in inadequate data for receiver function analysis. Hereafter, we use the term Moho depth as a representative of crustal thickness (H) below the station.

N-S section from Sana'a to Gulf of Aden

Crustal thickness for all the stations located on the plateau (SANA, YSLE, RUSA, DAMY and DAMT) is ranging between 35 and 35.4 km (Table 1, Fig. 3a). The identified Moho Ps conversion phase by the inversion appears between 4.83 and 4.93 s after the first

arrival (Fig. 3a). The associated *Vp/Vs* for these plateau stations ranges from 1.76 (RUSA) in the middle of plateau to 1.83 (DAMT) in the southern edge of the plateau. Such values are typical of felsic to intermediate composition crust (Christensen 1996). DAMT station is located in a hydrothermally active area resulting in deep circulation of the surface water, which is heated and returns back to the surface as steam and/or hot water (Fara *et al.* 1999; Alderwish & Almatary 2012). The high value of *Vp/Vs* for this station may be related to high porosity, the presence of water and gases in the upper few kilometres of sedimentary and volcanic rocks.

At some stations (e.g. SANA), a strong positive peak, attributed to an intra-crustal interface, can be observed before the Moho conversion Ps phase (Fig. 3a). For SANA station, we interpret this arrival as an intra-crustal discontinuity approximately located 21 km below the station (Figs 3–5). DAMY seems to have a shallower interface, as a similar peak is observed at 0.83 s delay time (<5 km depth, see Supporting Information).

KHLA has an estimated crustal thickness of ∼34 km (*Vp/Vs* of 1.75), slightly thinner than that to the north. The error estimate for this station is large (±6 and ±0.09 km for *H* and k, respectively) due to a weak Moho conversion phase Ps peak and numerous multiples for events approaching the station from the east. ADBA, further south, has a 31 km ±1.78 km thick crust associated with an average crustal *Vp/Vs* of 1.68 ±0.053 (Fig. 5).

The southern end of the profile is characterized by a thinner crust (23.6 and 20.4 km for DKUM and ADEN, respectively). These receiver functions also show a smaller amplitude Moho Ps conversion phase, implying a reduced impedance contrast across the Moho, especially for events approaching from the east (Figs 3a, 6b and 6d). The *Vp/Vs* are 1.69 and 1.73 for DKUM and ADEN, respectively. At ADEN station, we observe a high-amplitude intra-crustal conversion at 1.85 s (∼11 km) for all events with a backazimuth less than 106°N. This peak arrives earlier for more northerly azimuths as shown in Fig. (6b).

To further our understanding of the crustal layering along this section, we invert the receiver function waveforms for ADEN, ADBA, DAMT, RUSA and YSLE using the NA algorithm, as all of these stations show intra-crustal phases on their receiver function waveforms. Examples of inversion results are shown in Fig. (7). We obtain crustal thicknesses comparable to those from Zhu & Kanamori (2000) technique. ADBA has a complex crustal structure (Figs 4 and 8), with the inversion (Fig. 8) producing a low-velocity lower crust beneath the station, not observed on other stations. However, testing different forward models, the best fit is obtained for a model including a thin intra-crustal layer with both high *P*-wave velocity and *Vp/Vs* ratio (Figs 8c and d), rather than a low-velocity lower crust. We favour this model and interpret this high-velocity layer as a horizontal igneous intrusion (sill) into the crust.

For the Yemen permanent network stations located to the east of the N-S section of the profile (LBOS and BDHA, Fig. 2), we find 32.6 and 36.2 km crustal thickness with 1.83 and 1.76 *Vp/Vs* ratio, respectively. These values are consistent with the ones found for KHLA and ADBA.

E-W section from the Red Sea coast to Sana'a

The receiver functions of stations SHIB, TAWI, UAYA, ZUWA, ANID and MAWI are characterized by complex waveforms (Figs 3 and 4). For SHIB, TAWI and MAWI, the *H-k* stacking method gives a crustal thickness of 31.4 to 35.8 km, decreasing westward with a crustal *Vp/Vs* ratio around 1.8. Earlier peaks are observed at SHIB, MAWI (2.66 and 2.21 s, respectively) and to a lesser extend for

TAWI. They are interpreted as intra-crustal interfaces. We also note two later arrivals for these stations at about 6–8 and 10–11 s that cannot be modelled as multiples from shallower interfaces (Fig. 4). These are possibly upper mantle discontinuities, which need further investigation but are outside the remit of this paper.

On the sediments of the Tihama plain (ANID, ZUWA and UAYA), the receiver functions become more complex (Figs 3b, 4, 9b and 9c) due to conversions and multiples from the thick sediment layers, which include salt, covering the area. We stack 23 events for ANID station, located at the eastern end of Tihama coastal plain and observe three positive peaks at 1.75, 3.3 and 6.95 s delay times (Fig. 4). The first peak is interpreted as an intra-crustal phase, and in this case, the third one could be a multiple of the first; the second one is interpreted as the Moho conversion phase. It gives a crustal thickness of 22.8 km and a *Vp/Vs* value of 1.83 (Figs 4 and 5).

ZUWA station shows two main features. First, the low amplitude of the first P compared to the following Ps conversion (Fig. 9c) comes from the sediment-bedrock interface beneath the station. Second, we observe a clear shift of Moho Ps conversion between events with easterly backazimuths (<106°) and events with westerly backazimuths (>140°). We can explain this by ZUWA being located near a N-S normal fault, implying an azimuth-dependent velocity structure. For azimuths <106°, seismic structure will be similar to the ANID case (*Vp* = 6.2 km s⁻¹), whereas for azimuths >140°, it will be similar to UAYA station. For the latter case, we base our choice on Egloff *et al.* (1991) study (profile VI) and take an average *Vp* of 5.3 km s⁻¹ (4 km of sedimentary layer). We then proceed with two separate inversions, and in both cases, we obtain a best-fit result for a crustal thickness of 23 km, consistent with the value obtained for the nearby station ANID. The corresponding *Vp/Vs* ratios are 1.91 and 1.95 for azimuths >140° and <106°, respectively (Fig. 9c). These are the highest values of *Vp/Vs* ratio we obtain for all the stations. We relate it to sedimentary deposits in Tihama basin (Egloff *et al.* 1991; El-Anbaawy *et al.* 1992; Davison *et al.* 1994).

UAYA, located along the Red Sea coast, has numerous high-amplitude conversion phases prior to the Moho Ps within a very small time window of 2.27 s (Fig. 9b). However, there are two dominant conversion phases one at 1.3 s and the other at 2.3 s, with multiples at 5.3, 6.6, 7.3, 10 s, respectively. The first one is a conversion phase at an intra-crustal interface at about 9.6 km depth when using an average upper crustal velocity *Vp* of 4.5 km s⁻¹ (Egloff *et al.* 1991), while the second one is the Moho conversion phase. Based on our estimate of the average velocity for the crust from the results of seismic profile VI of Egloff *et al.* (1991) near the coast of the Red Sea, we obtain a crustal thickness of 13.8 km with a *Vp/Vs* ratio of 1.92 (*Vp* = 5.3 km s⁻¹).

Stations adjacent to the Red Sea coast

For the Red Sea coast stations SUGH, KHAW and MOKA (Fig. 2), we find a consistent crustal thickness estimate varying 21.5–23.2 km (Table 1). The estimated *Vp/Vs* for these three stations is 1.73, 1.68 and 1.85, respectively. KHAW station has the lowest *Vp/Vs* ratio of the three (1.68). Sedimentary layering likely affects KHAW signal (trough at 2,s following the positive peak at 0.5 s, Figs 3c and 4). The MOKA receiver function contains two high-amplitude Ps conversions at 1.2 and 1.88 s (Fig. 3c). The first conversion occurs at the base of a low-velocity sediment layer. The second conversion corresponds to the interface between the upper and lower crust modified by high-velocity mafic intrusion (*Vp/Vs* = 1.85). The
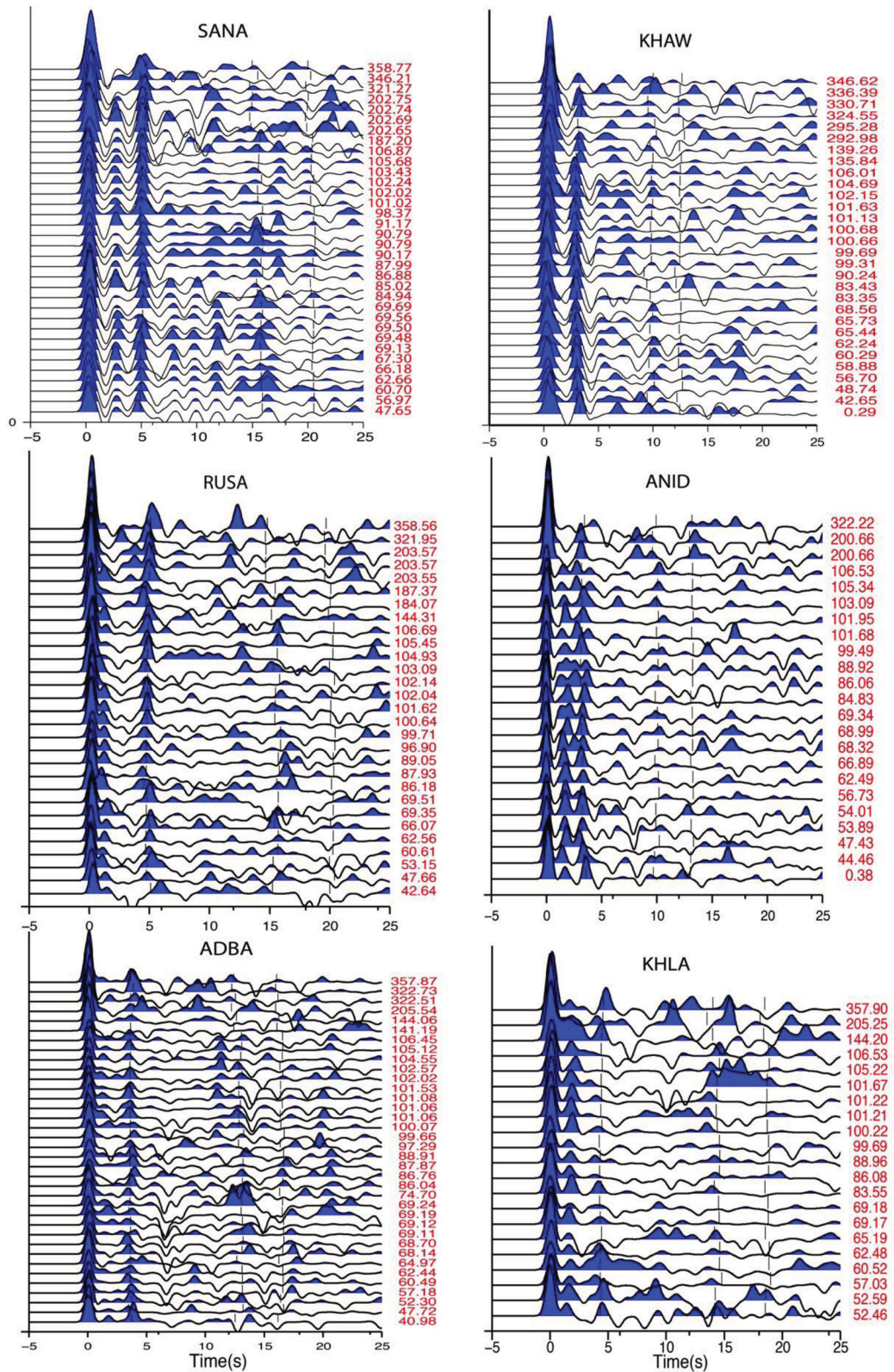
Figure 4. Receiver functions for six stations of the profile. The receiver functions are organized by increasing backazimuth (red number right of the trace). The light vertical lines indicate arrival times for conversion phases (Ps and multiples) from the Moho for the maximum stacking amplitude.

Moho Ps conversion phase is very low amplitude at this station, and thought to be due to a reduction in the impedance contrast across the boundary from the presence of the high-velocity lower crust (HVLC).

For TRBA station, we estimate the crustal thickness to be 27.4 km with a *Vp/Vs* ratio of 1.86. A shallow interface can also be deduced from a weak amplitude Ps conversion at 0.85 s delay time (Fig. 3d), while the interface between the upper and lower crust cannot be
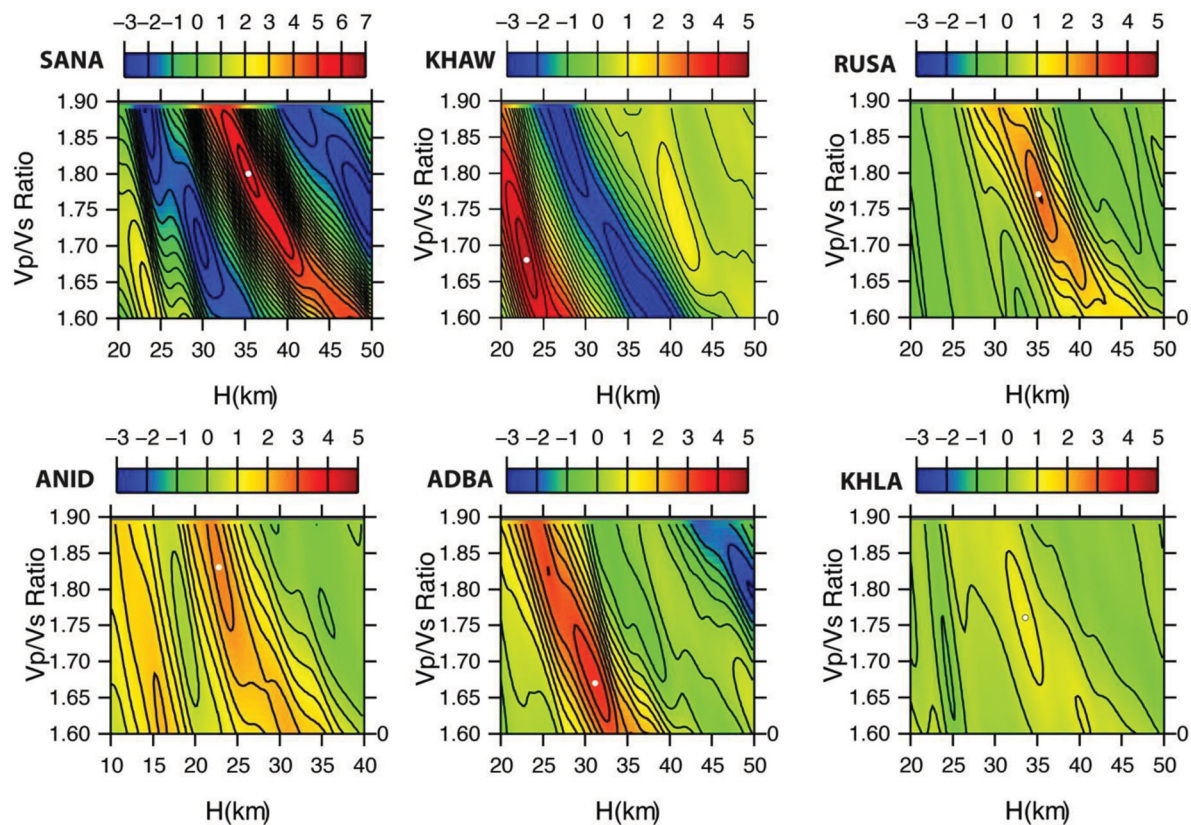
Figure 5. Thickness (*H*) versus *Vp/Vs* ratio diagrams from the *H-k* stacking method for six of our stations in Fig. 4. The maximum of the stacking amplitude is indicated by the white point and corresponds to the value indicated in Table 1. The scale bar is the amplitude of stacking function.

seen. This is comparable to the results of the stations located on the volcanic trap series south of SANA.

Imaging the crustal structure by migration of receiver functions

Migration of receiver functions from the time domain to the space domain is a common technique to image the continuous variations of the structures beneath a receiver function profile (e.g. Kind *et al.* 2002). In this study, we use the common conversion point (CCP) stacking technique of Zhu (2000). A bin size of 20 km wide, 5 km long and 0.5 km vertically is used. These parameters have been chosen in order to optimise both resolution of the interfaces and their spatial continuity. The migrated cross sections have been created using IASP91 velocity model (Kennett & Engdahl 1991). Fig. 10 displays the migrated receiver functions along the N-S and E-W sections. As a comparison, the inverted Moho depth (referred to sea level) using the *H-k* stacking method of Zhu & Kanamori (2000) is plotted as black dots with error bars using the bootstrap technique.

The Moho discontinuity is associated with a strong positive amplitude (red colour; Fig. 10), which diminishes in amplitude as one moves towards the coast. For the N-S profile, the Moho interface is sub-horizontal between SANA and DAMT at an approximate depth of 35 km. At the southern end of the profile, the Moho is at a depth of ~20 km beneath ADEN. Between ADBA and DKUM, ~7.5 km of crustal thinning happens over 32 km lateral distance. The intra-crustal interface between 15 and 21 km, interpreted here to be the upper/lower crust boundary, is observed between SHIB and SANA, and then between DAMT and ADBA stations. The change in the

character of this intra-crustal boundary between SANA and DAMT may be explained by lateral variations in crustal composition.

In the E-W-migrated receiver function profile, the Moho discontinuity is clear and lies at a depth of 35 km at the eastern end of the profile. It then rises steeply in two stages at the western end to reach ~14 km beneath UAYA. The first stage of crustal thinning occurs between MAWI and ANID (~8.6 km vertically over 34 km horizontally). The second stage of thinning comes between ZUWA and UAYA (~9.2 km vertically over 30 km horizontally). A clear positive phase is observed along the section in the east from 21 km depth (SANA) up to 9.6 km (UAYA), which corresponds to a clear crustal conversion in the signal at all stations. This conversion is weak at TAWI and is smeared between TAWI and MAWI (see individual RFs in Supporting Information). We interpret it to be the interface between the upper and lower crust.

DISCUSSION

Thinning of the crust

Our crustal thickness estimates range between 20 and 23 km in the coastal areas to 35–36 km below the Yemen plateau. These are comparable to the results from other studies of the western Arabian Plate shown in Fig. 11 (Mooney *et al.* 1985; Al-Damegh *et al.* 2005; Hansen *et al.* 2007). Exceptionally. thin crust of ~14 km is observed beneath UAYA right on the Red Sea coast.

The 1988 SONNE seismic line from the Red Sea coast to the Yemen plateau estimated the crust to be 4–8 km thicker in the coastal areas and ~9 km thinner below the plateau than we achieve here
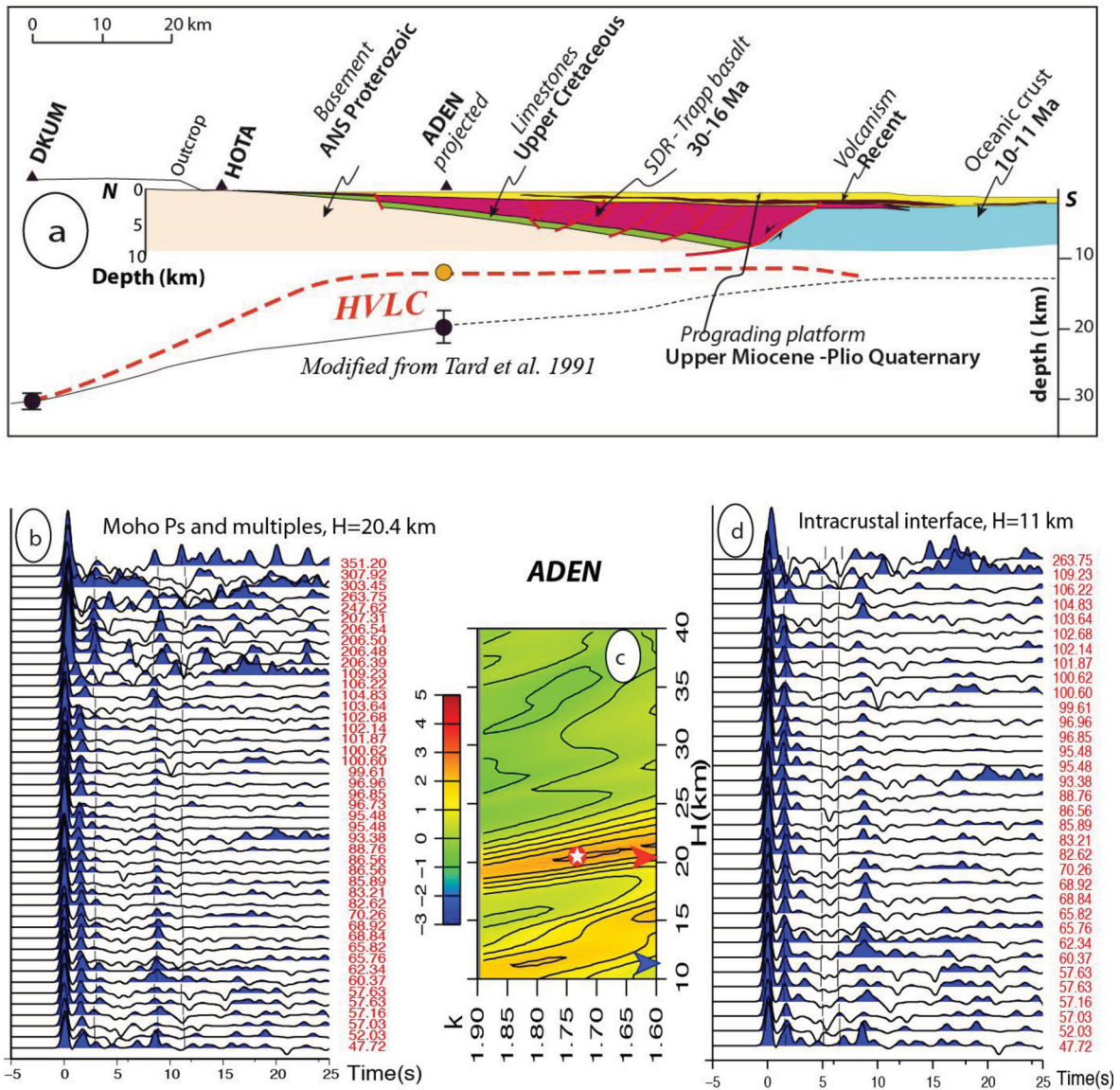
Figure 6. RF and cross-section western Gulf of Aden volcanic margin. (a) cross section showing Moho depth and HVLC from our results and the interpretation of seismic line after Tard *et al* .(1991). (b) RF of ADEN station with vertical lines showing the Moho conversion phase and multiples. (c) Crustal thickness *H* versus *Vp/Vs* ratios, scale bar is the amplitude of the stacking function, white star is the maximum of the *H-k* plot, red arrow pointing to the Moho depth and blue arrow showing the depth of HVLC. (d) RF with vertical lines showing HVLC conversion phase and multiples. The RFs are annotated by red numbers (backazimuth).

using receiver function analysis (Egloff *et al.* 1991, Fig. 2). Makris *et al.* (1991), from a gravity interpretation, estimate the crust to be 35 km below Sana'a and 22 km below Tihama plain, which is consistent with our results, and also implies that the entire area is isostatically compensated.

Our crustal thickness beneath the Yemen Plateau (∼35 km) corresponds to the lower bound of the Ethiopian Plateaus crustal thicknesses (between 35 and 45 km, Stuart *et al.* 2006; Bastow *et al.* 2011; Hammond *et al.* 2011) (Fig. 11). Our lowest value beneath UAYA (∼14 km) is very close to the one obtained in the Danakil depression (Bastow & Keir 2011; Hammond *et al.* 2011; Keir *et al.* 2012) (Fig. (11)), where mafic intrusions feeding volcanism are also likely to take place (e.g. Tiberi *et al.* 2005; Field *et al.* 2012; Nobile *et al.* 2012).

There is a clear mid-crustal interface at depths between 10 and 21 km along the E-W profile (Fig. 10) as well as at stations located to the east of Yemen volcanic trap series (DAMT, KHLA, ADBA, LBOS and BDHA). We interpret this interface to be the upper/lower crust boundary—the Conrad discontinuity. This discontinuity is caused by a sharp velocity step separating the upper crust (average *Vp* of 6.3 km s^{-1}) from the lower crust (average *Vp* of 7.0 km s^{-1}) (e.g. Mooney *et al.* 1985; Egloff *et al.* 1991). Such an interface is a common feature in the Arabian plate (Mooney *et al.* 1985; Egloff *et al.* 1991; Stern & Johnson 2010). Stern & Johnson (2010) suggest that it separates slower felsic upper crust from faster mafic lower crust, and may coincide with the transition from brittle to ductile deformation. For those stations located on the Yemen volcanic trap series (YSLE, RUSA, DAMY and TRBA), south of Sana'a (Fig. 10)
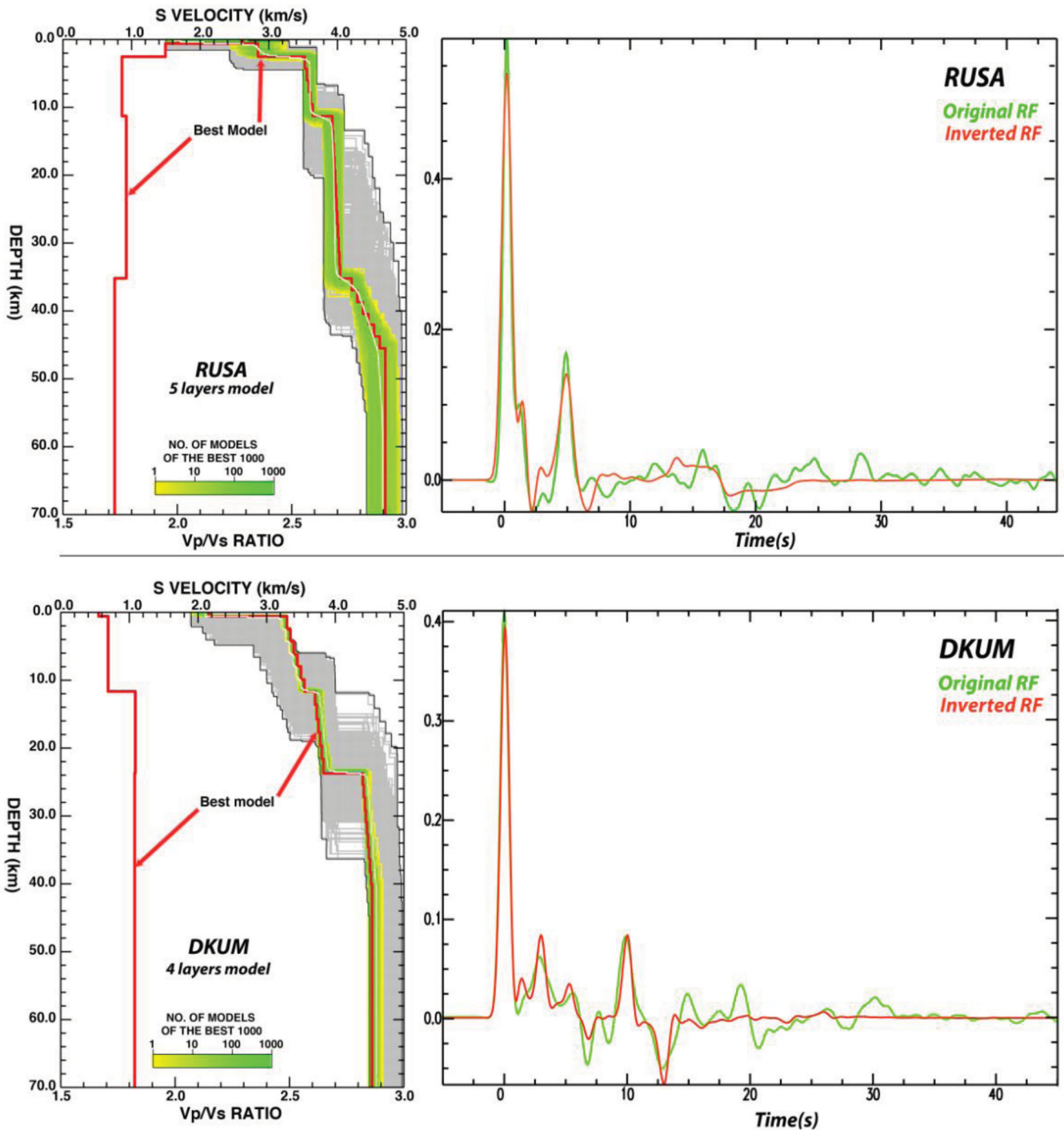
Figure 7. (Left) Seismic velocity models for RUSA and DKUM stations obtained from the neighbourhood algorithm method (Sambridge 1999a). The grey area indicates all the models searched by the algorithm. The best 1000 models are indicated in yellow–green colour, the best one (smallest misfit) corresponds to the red line, both for *S*-wave velocity and *Vp/Vs* ratio and the white line is the average velocity model. (Right) Waveform matches between the observed stacked receiver functions (green) and the predicted one (red) based on the best models (red lines in the left-hand diagrams).

and also KHAW on the Red Sea coast, the Conrad discontinuity is not imaged by our receiver functions. This implies that the crust was modified by magma intrusion during the Oligo-Miocene flood basalt volcanism caused by the impact of the Afar plume ∼30 Ma ago (Baker *et al.* 1994), and decompression melting of hot mantle during rifting. The shallower interface below those stations (1–

4 km depth) is interpreted as the boundary between basement and the overlaying thick sedimentary and/or volcanic cover.

The onset of crustal thinning on the Gulf of Aden margin starts somewhere between KHLA and DAMT and ends between ADBA and DKUM (Fig. 10). This implies one stage of thinning (7.4 km vertically over 32 km horizontally). If we assume the average initial
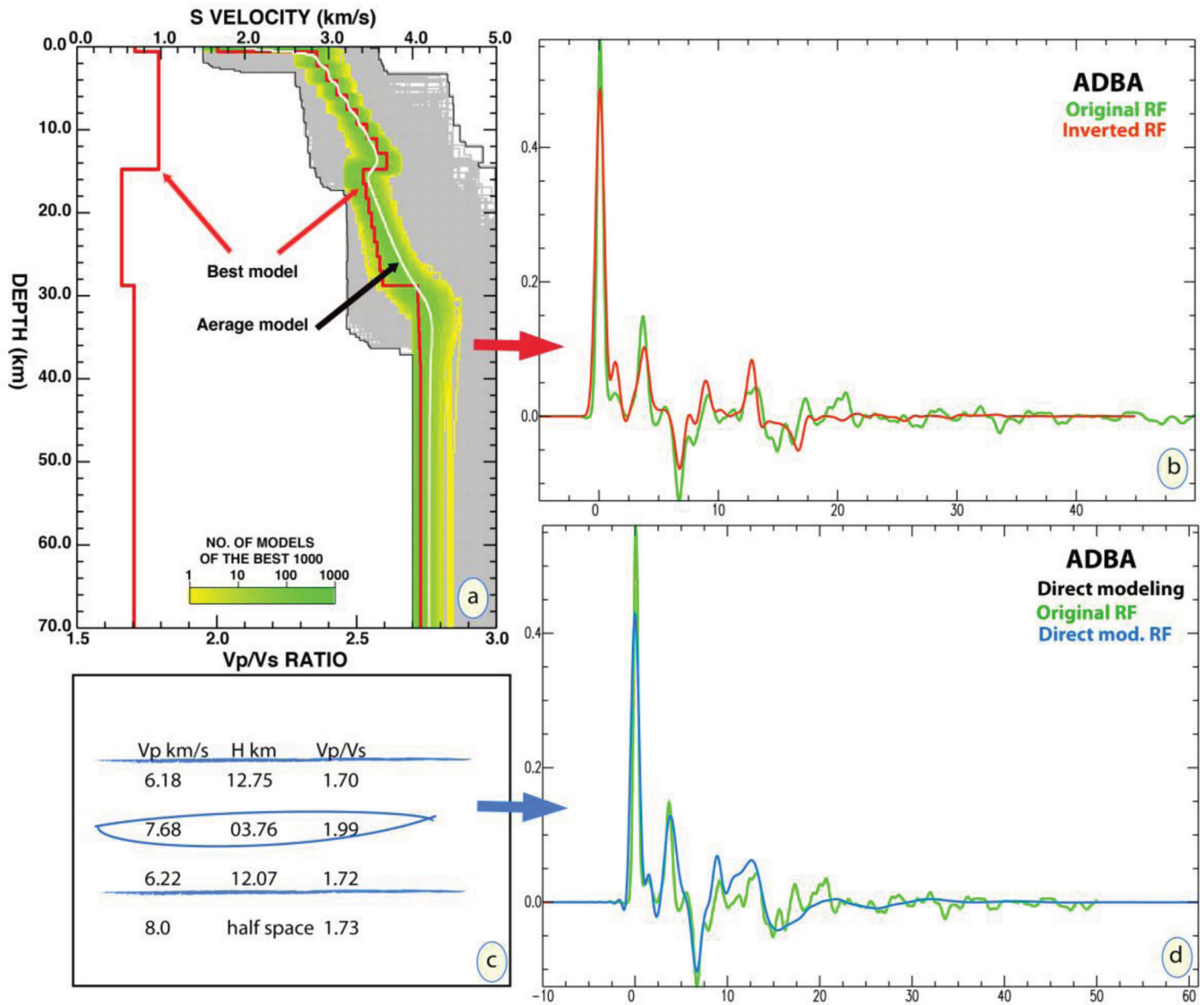
Figure 8. Neighbourhood algorithm (NA) inversion and direct modelling results for ADBA. (a) Velocity models explored with the NA inversion. The best model is indicated with the red line and corresponds to the red receiver function signal in (b). (c) Velocity model used to obtain the dark blue modelled receiver function in (d).

crustal thickness to be 35 km (SANA) and the final extended crust for the coastal areas to be 22 km (ADEN), the corresponding β stretching factor is around 1.6. This value gives a lower bound estimate of the stretching factor since mafic intrusions maintain crustal thickness during extension. An upper bound for the stretching factor is obtained by only considering the upper 12 km as non-intruded crust beneath ADEN, which yields $\beta \sim 3$.

On the Red Sea margin, however, the history of extension is likely more complex. If we consider the extended crustal thickness to be that of UAYA (13.8 km), we obtain a stretching factor as high as 2.5, which is slightly higher than the maximum value reported beneath the Red Sea, offshore Yemen ($\beta \approx 2.4$, Davison *et al.* 1994). Moreover, we observe two step changes in the crustal thickness (Figs 9 and 10). The first step is observed between the plateau ($h \sim 35$ km) and the coastal plain ($h \sim 22$ km). The second step is located between ZUWA and UAYA stations, where the crustal thickness decreases sharply from $h \sim 22$ km at the coastal plain to 13.8 km at UAYA over ~ 30 km. The lower bound of β factor

estimate is estimated at ~ 1.6 for both steps in crustal thickness, similar to the Gulf of Aden margin, and comparable with the results for the stretching factor calculated from geometry of fault block rotations (Davison *et al.* 1994). When comparing the 35-km-thick non-extended crust beneath SANA and the present 14 km beneath UAYA, we obtain a maximum β of 2.5. A similar value of 2.4 is obtained between UAYA and ZUWA when considering that mafic intrusion maintained the crustal thickness and thus overestimates its value beneath UAYA (14 instead of 9.6 km). Our results suggest that two stages of crustal extension should be then considered for the Red Sea margin.

Crustal underplating (HVLC)

On the Red Sea coast UAYA has a strong intra-crustal interface at 9.6 km depth with clear multiples, and a Moho discontinuity at about 13.8 km depth (Fig. 9). Our crustal thickness estimate is consistent with the 11–14 km obtained further south near Al-Hudaidah
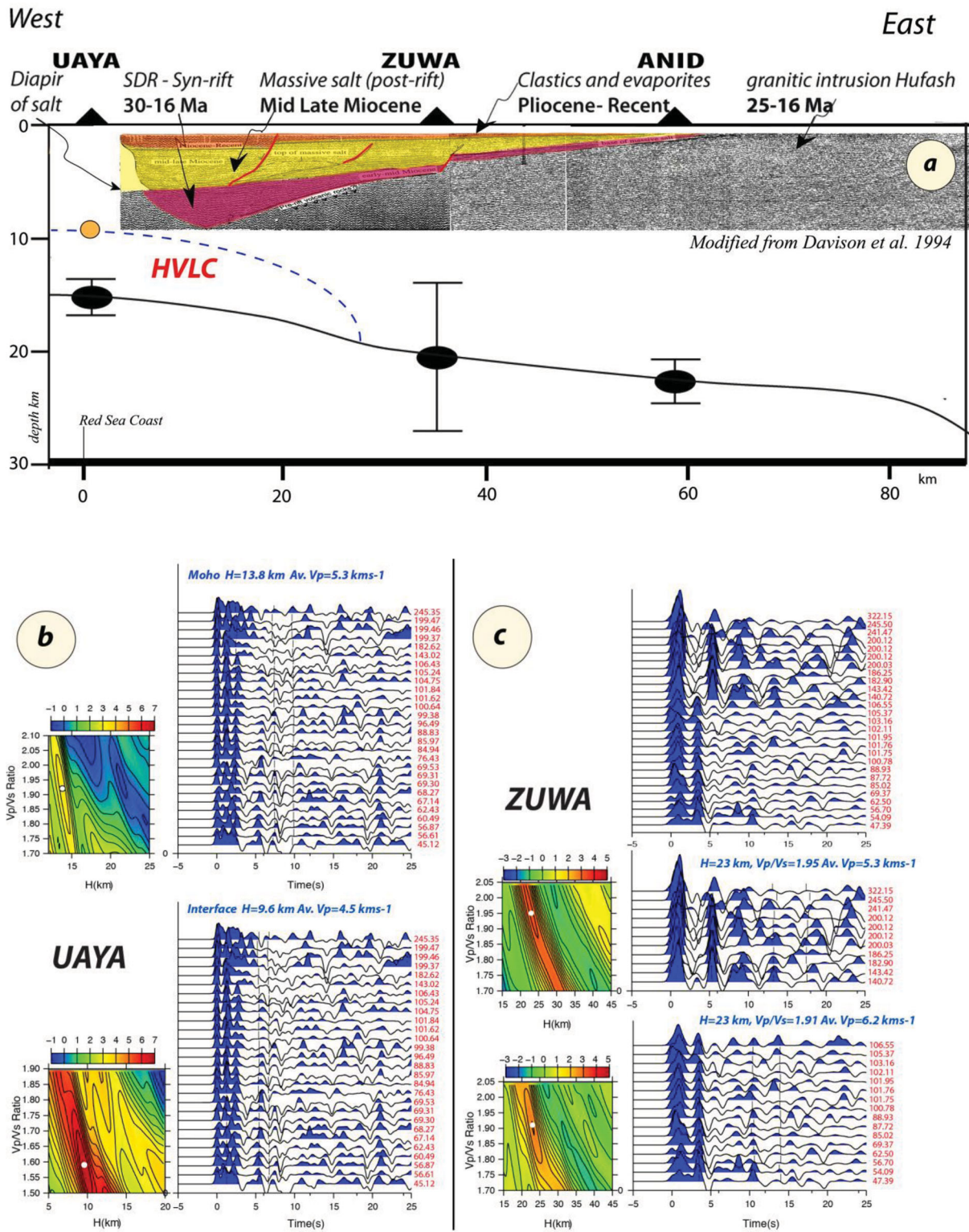
Figure 9. Receiver function (RF) and cross-section across the Red Sea volcanic Margin. (a) Cross section of Moho discontinuity and the HVLC, with the projection of seismic line after Davison *et al.* (1994). (b) RF and H versus *Vp/Vs* ratio diagrams from *H-k* stacking results for UAYA station. Vertical lines show the Moho conversion phase and multiples top and HVLC conversion phase with multiples bottom. (c) RF and *H* versus *Vp/Vs* diagrams for ZUWA station. (Top) ZUWA RF organized by increasing backazimuth as indicated by red numbers to the right. (Middle) RF for backazimuth range >140° and (bottom) RF for backazimuth < 106°. Crustal thickness, *Vp/Vs* ratio and average crustal *Vp* used for inversion are marked by blue text in the RF figures. Scale bar is the amplitude of the stacking function.
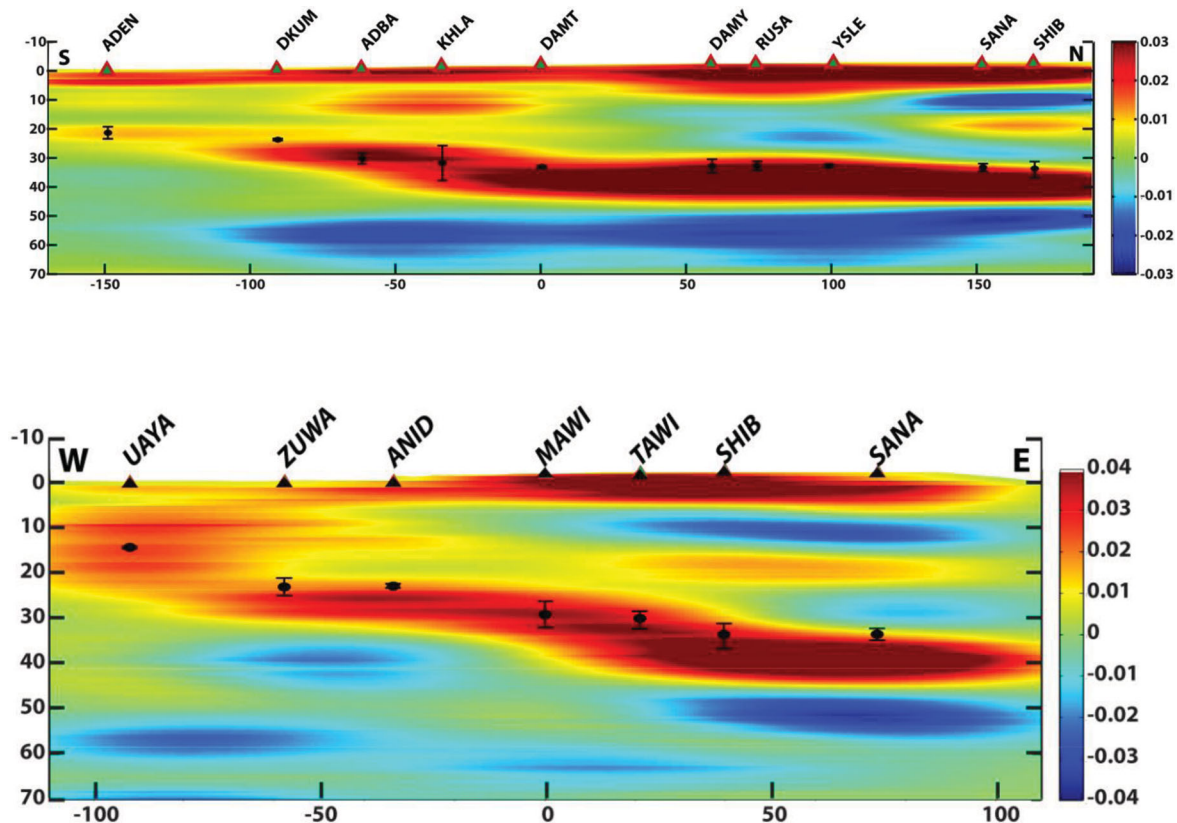
Figure 10. Migrated cross-sections following the main profile sections, E-W (bottom centred at MAWI oriented N100E) and N-S (top centred at DAMT oriented NS). The Moho depth estimated from *H-k* stacking method is plotted with the black dots with error bars from bootstrap. Red colour indicates velocity increase with depth, and blue colour velocity decrease with depth. Scale bar shows the amplitude of positive (red) and negative (blue) polarities of arrivals.

(Fig. 2) during the SONNE experiment (Egloff *et al.* 1991). Considering local isostasy with an average crustal density of 2670 kg m^{-3} and a mantle density of 3300 kg m^{-3}, the Moho should be at ∼22-km-depth beneath UAYA. The presence of SDRs in this region (Davison *et al.* 1994) and our results of two conversion phases and multiples suggest the presence of a HVLC (Fig. 9). Consequently, we conclude that the area is underplated by a high-velocity dense material resultant from the ∼11 Ma rifting episode (Eagles *et al.* 2002). This explains both a thinner crust and the complexity of the signal beneath UAYA. North of UAYA at the western end of the Saudi Arabian refraction profile (between shot point 5 ∼17.77 N, 42.35 E and shot point 6∼16.57 N, 42.06 E), there is evidence of a double-layered Moho overlain by a sedimentary basin containing salt deposits (Milkereit & Flüh 1985; Mooney *et al.* 1985; Prodehl 1985). Further south along the Red Sea coast, there is no evidence of a similar HVLC either from the controlled source seismic profile near Al-Hudaydah (Egloff *et al.* 1991) or from our receiver function results at KHAW. However, at MOKA (Fig. 2), a complex receiver function is found similar to that at UAYA with high-amplitude intra-crustal multiple conversion phases and a low-amplitude Moho Ps conversion phase with its associated multiples (Fig. 3c). This receiver function waveform together with the existence of Miocene volcanism in Jabal An Nar near MOKA (Capaldi *et al.* 1987) may indicate the presence of local underplating. Such isolated off-axis underplated volcanoes have been reported at eastern Gulf of Aden continental margin (Lucazeau *et al.* 2009; Autin *et al.* 2010; Watremez *et al.* 2011).

On the Gulf of Aden coast, we interpret the intra-crustal interface we found at 11 km (Fig. 6) to be an intrusion of igneous material at the base of the lower crust. This causes weak impedance contrast between the lower crust and the mantle, thus explaining the low-amplitude Moho Ps conversion phase observed (Fig. 6). However, this HVLC produces a high-impedance contrast with the overlying upper crust, causing the high-amplitude conversion phase we observe at ∼2 s in Fig. 6. The thickness of the HVLC works out to be ∼9 km from these observations. Tard *et al.* (1991) identified syn-rift SDRs in this area. We thus conclude that this margin is a typical volcanic margin (e.g. Leroy *et al.* 2012).

Our observations and previous studies (volcanism, tectonics, geochronology; e.g. Bosworth *et al.* 2005) suggest that the onset of rifting along the western Gulf of Aden and the southern Red Sea was synchronous. From our results of the crustal thickness in UAYA, we propose a second phase of thinning confined to the Red Sea which has been suggested in previous studies (e.g. Girdler & Styles 1974). This rifting phase could have occurred after the deposition of the halite deposits and during the initiation of new oceanic crust in the southern end of the Red Sea axial trough (Egloff *et al.* 1991), and related to a mantle exhumation phase (Leroy *et al.* 2010b). Dating the timing of the halite deposition (syn or post-rift, Fig. 9) and the Yemeni granite intrusions (Hughes & Beydoun 1992; Davison *et al.* 1994; Geoffroy *et al.* 1998, Fig. 2) would clarify the timing of rifting phases.

The crustal characteristics of the western Yemen volcanic rifted margin can be recognized in other volcanic margins (Menzies *et al.*
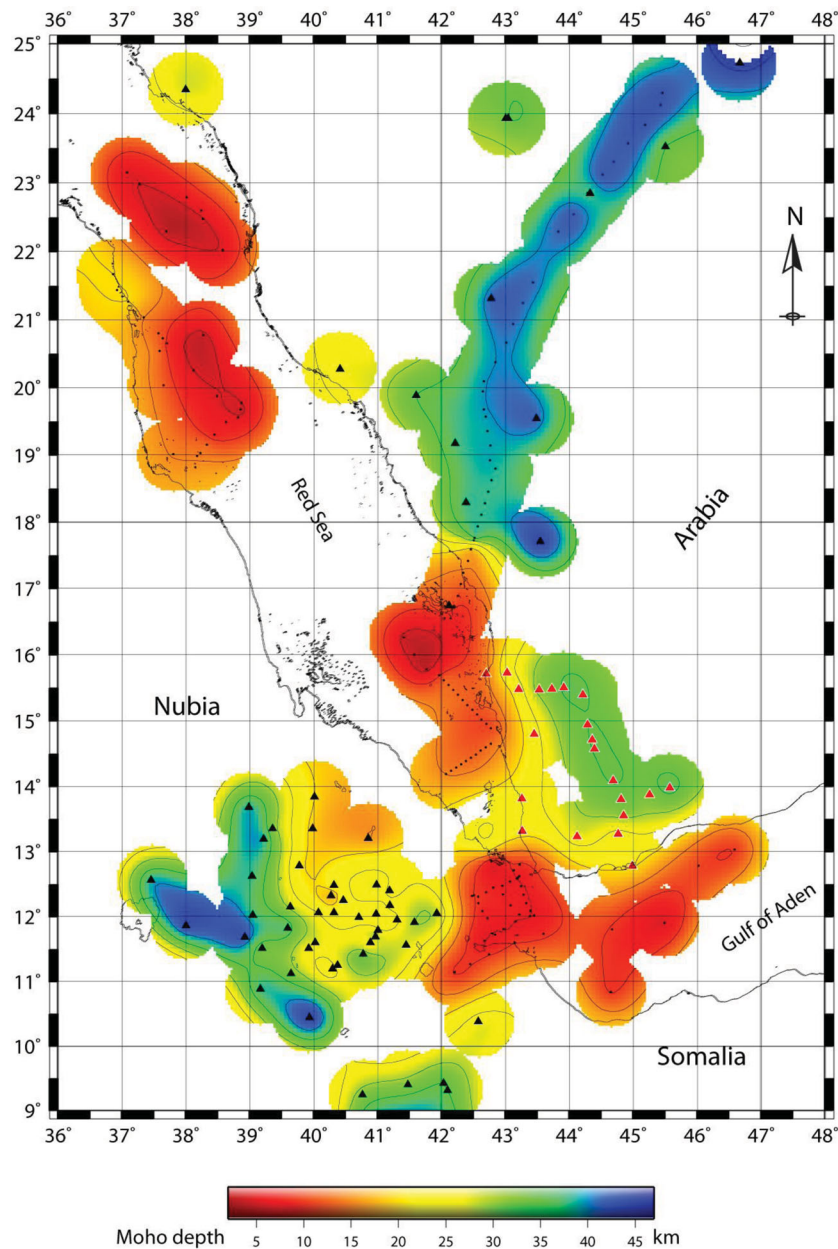
Figure 11. Regional map showing Moho depths (below sea level) based on the results of this study (red triangles) and previous RF studies (black triangles) in Ethiopia (Hammond *et al.* 2011), and Saudi Arabia (Hansen *et al.* 2007), active seismic studies (black dots) in the Red Sea (Drake & Girdler 1964; Tramontini & Davies 1969; Egloff *et al.* 1991; Prodehl & Mechie 1991), controlled source study in the Western Gulf of Aden (Laughton & Tramontini 1969), seismic refraction profiles in Djibouti (Ruegg 1975) and Saudi Arabian seismic refraction profile (Mooney *et al.* 1985).

2002; Direen *et al.* 2008). (1) The pre-rift Oligio-Miocene flood basalt volcanism (Yemen Trap Series), which could be related to Afar plume activity at ~30 Ma, is similar to south Atlantic volcanic margins with the emplacement of pre-rift Paraná-Etendeka flood basalt, for example, the Namibia volcanic margin (Gladczenko *et al.* 1998); (2) A 50–70 km wide volcanic margin transition zone from extended and intruded continental crust to true oceanic crust is similar to that observed at volcanic margins of the North Atlantic such as the Hatton Bank volcanic margin (Smith *et al.* 2005), and the narrower 10–40 km wide extended zone reported for Møre volcanic margin (Mjelde *et al.* 2009). In the South Atlantic (Nambia) and offshore western Australia, wider ~150–200 km extended zones have been interpreted (Gladczenko *et al.* 1997; Gladczenko *et al.*

1998; Bauer *et al.* 2000; Direen *et al.* 2008); (3) On the eastern coast of the Red Sea, most of the syn-rift and post-rift mafic dykes, which parallel the Red Sea margin, are concentrated along the Tihama plain escarpment area (Mohr 1991). On the plateau, in the Aden traps of Dhala, Musaymir and Radfan, the dike trends are variable from NW to NE (Moseley 1969; Mohr 1991), while most of the dykes along Aden volcanic line are in an EW direction parallel to the Gulf of Aden rift (Cox *et al.* 1970); (4) In the Gulf of Aden, SDRs overlie most of the extended zone and thicken seaward (Tard *et al.* 1991; Leroy *et al.* 2012). SDRs are one of the distinguishing features of volcanic margins and have been imaged in seismic profiles at the Labrador Sea (Keen *et al.* 2012), Namibia (Bauer *et al.* 2000) and Exmouth–Gascoyne margin western Australia (Rey *et al.* 2008)

volcanic margins. (5) HVLC (underplating) is an important feature of volcanic margins and has been identified for both the Red Sea and Gulf of Aden margins (e.g. Milkereit & Flüh 1985; Prodehl 1985). HVLCs exist in Exmouth–Gascoyne, Namibia, Møre, Hatton Bank and Vøring typical volcanic margins (Bauer *et al.* 2000; Gernigon *et al.* 2004; Smith *et al.* 2005; Rey *et al.* 2008; Mjelde *et al.* 2009). (6) Oceanic crust at the axial trough of Red Sea and along Gulf of Aden spreading center has been reported by many studies (e.g. Girdler & Underwood 1985; Bosworth *et al.* 2005; Leroy *et al.* 2012). In the Red Sea, 4-km-thick oceanic crust is reported in the central part of the axial trough and 1–3 km thick of new oceanic crust is estimated for the southern part north of 15.5° N latitude (Egloff *et al.* 1991; Girdler 1991). For the Gulf of Aden, the oceanic crust is thicker (∼8 km) and covers a wider area on either side of the oceanic ridge chron A5d (∼17.6 Ma) in the east of Shukr-Alsheik fracture zone and A4a (∼9 Ma) in the south of Aden (Hébert *et al.* 2001; Leroy *et al.* 2012).

Vp/Vs ratio and crustal composition

Most of the stations are characterized by felsic to intermediate composition crust with Vp/Vs in the range of $1.73 \leq k \leq 1.86$ (Christensen 1996) (Table 1). This average Vp/Vs is for the bulk crust. However, the mid-crustal discontinuity suggests a mafic composition for the lower crust in particular, which has been altered by magmatism during Miocene-Oligocene times. It is difficult to determine how the lower crust has been altered, whether by intruded material originating from the mantle or by an alternative alteration process (Baker *et al.* 1998) given only Vp/Vs ratios. However, the seismic refraction profiles in Saudi Arabia and Yemen confirm this crustal division and show an average Vp of 6.3 km s^{-1} for the upper crust and 7.0 km s^{-1} for the mafic lower crust (Mooney *et al.* 1985; Egloff *et al.* 1991). Stern & Johnson (2010) described the lower crust beneath Arabian shield to be broadly gabbroic in composition with the possibility of second-order compositional variations such as increased plagioclase content upwards and increased pyroxene content downwards. They also concluded that most of the Arabian shield upper crust was formed by magmatic additions at intra-oceanic arcs above past subduction zones (870–630 Ma) with post-tectonic subordinate granitic and volcanic rocks contributing to the growth of the Arabian shield.

Hammond *et al.* (2011) ascribed the Vp/Vs ratio variation (1.7–1.9) for western Ethiopian plateau to mafic crust altered by the Cenozoic volcanism, whereas the south-eastern plateau shows more typical silicic continental crust with a Vp/Vs ratio of 1.78. Dugda *et al.* (2005) concluded that the crustal structure on the western side of Ethiopian plateau has not been altered by Cenozoic volcanism as the Moho depth and average Vp/Vs ratio are comparable to unmodified Mozambique Belt crust in Tanzania and Kenya and similar to the global average for Precambrian crust. Our results from the Yemen plateau show that low Vp/Vs values (∼1.68) characterise stations located on the granitic intrusions or on the Precambrian quartz-rich rocks.

For the Red Sea coastal area west of ZUWA station, the Vp/Vs ratio is greater than 1.90. High values in this area could reflect sedimentary infill (Fig. 9). The presence of a HVLC beneath UAYA increases the Vp/Vs ratio (1.92) due to its mafic nature (Watanabe 1993; Christensen 1996). The complex receiver function in the presence of a HVLC and the high Vp/Vs ratio values near the Red Sea coast provides strong evidence for a different amount of extension in this area. In contrast, the lower Vp/Vs of 1.73 for ADEN station is not expected in a basalt volcanic field. This low Vp/Vs value might suggest the existence of water in the crust. Watanabe (1993) concluded that as the fluid fraction increases to 10 vol. per cent in case of water, the Vp/Vs will decrease though in case of molten rocks it will increase.

CONCLUSION

From a detailed study of the receiver functions through a profile in Western Yemen, we were able to:

1) map the Moho depth variations both for the Gulf of Aden and Red Sea margins. The crustal thickness beneath the Yemen Plateau is ∼35 km consistent with values obtained elsewhere in the interior of the Arabian peninsula. The thickness decreases to 22 km for the coastal regions of the Aden rift and to less than 15 km for the Red Sea. The lower-bound stretching factors we deduced are ∼1.6 for both rifts, implying a coeval rifting history, except in the UAYA region where our results strongly suggest that a second phase of rifting with the same stretching factor has occurred after the deposition of halite deposits.

2) image intracrustal discontinuities beneath a number of stations in Yemen. One of these interfaces at ∼10–21 km depth is interpreted as the Conrad discontinuity, separating the upper from the lower crust. It is particularly well imaged beneath the stations located along the E-W section and is not visible in regions of extensive volcanism to the east. Near the coastal areas, the shallowest interfaces may be related to the sediment-basement contact.

3) confirm that the volcanic margins of western Gulf of Aden and southern Red Sea are underplated by high-velocity dense material at the base of lower crust (HVLC). The HVLC is overlain in the upper crust by SDRs evidenced in previous seismic profiling studies.

4) estimate Vp/Vs ratios of 1.73–1.86 indicative of altered mafic lower crust and felsic upper crust beneath the plateau and southern part of the profile. For those stations located on or near granitic bodies, the crust is more silicic. Regions overlain by sedimentary basins have modified thinned lower crust.

REFERENCES

Al-Dameeh, K., Sandoval, E. & Brazangi, M., 2005. Crustal structure of the Arabian plate: new constraints from the analysis of teleseismic receiver functions, *Earth planet. Sci. Lett.,* **231,** 177–196.

Alderwish, A. & Almatary, H., 2012. Hydrochemistry and thermal activity of Damt region, Yemen, *Environ. Earth Sci.,* **65**(7), 2111–2124.

Ammon, C.J., 1991. The isolation of receiver effects from teleseismic P waveforms, *Bull. seism. Soc. Am.,* **81,** 2504–2510.

Ammon, C.J., Randall, G. & Zandt, G., 1990. On the nonuniqueness of receiver function inversions, *J. geophys. Res.,* **95,** 15 303–15 318.

Autin, J. *et al.*, 2010. Continental break-up history of a deep magma-poor margin from seismic reflection data (northeastern Gulf of Aden margin, offshore Oman), *Geophys. J. Int.,* **180,** 501–519.

Baker, J., Menzies, M. & Snee, L., 1994. Stratigraphy, 40Ar/39Ar geochronology and geochemistry of flood volcanism in Yemen, *Mineral. Mag.,* **58A,** 42–43.

Baker, J., Chazot, G., Menzies, M. & Thirlwall, M., 1998. Metasomatism of the shallow mantle beneath Yemen by the Afar plume.implications for mantle plumes, flood volcanism, and intraplate volcanism, *Geology,* **26,** 431–434.

Bastow, I.D. & Keir, D., 2011. The protracted development of the continent–ocean transition in Afar, *Nat. Geosci.,* **4**(4), 248–250.

Bastow, I.D., Keir, D. & Daly, E., 2011. The Ethiopia Afar Geoscientific Lithospheric Experiment (EAGLE): probing the transition from continental rifting to incipient seafloor spreading, *Geol. Soc. Am. Spec. Pap.,* **478,** 51–76.

Basuyau, C., Tiberi, C., Leroy, S., Stuart, G., Al-Lazki, A., Al-Toubi, K. & Ebinger, C., 2010. Evidence of partial melting beneath a continental margin: case of Dhofar, in the Northeast Gulf of Aden (Sultanante of Oman), *Geophys. J. Int.,* **180,** 520–534.

Bauer, K. *et al.*, 2000. Deep structure of the Namibia continental margin as derived from integrated geophysical studies, *J. geophys. Res.,* **105,** 25 829–25 853.

Beydoun, Z.R., 1997. Introduction to the revised Mesozoic stratigraphy and nomenclature for Yemen, *Mar. Petrol. Geol.,* **14,** 617–629.

Bosworth, W., Huchon, P. & McClay, K., 2005. The Red Sea and Gulf of Aden basins, *J. Afr. Earth Sci.,* **43,** 334–378.

Buck, W.R., Einarsson, P. & Brandsdottir, B., 2006. Tectonic stress and magma chamber size as controls on dike propagation: constraints from the 1974–1989 Krafla rifting episode, *J. geophys. Res.,* **111**(B12), B12404, doi:10.1029/2005JB003879.

Burdick, L.J. & Langston, C.A., 1977. Modeling crustal structure through the use of converted phases in teleseismic body waveforms, *Bull. seism. Soc. Am.,* **67,** 677–692.

Capaldi, G., Manetti, P., Piccardo, G.B. & Poli, G., 1987. Nature and geodynamic significance of the Miocene dyke swarm in the North Yemen (YAR), *Neues Jahrb. Mineral. Abh.,* **156,** 207–229.

Chang, S.-J. & Van der Lee, S., 2011. Mantle plumes and associated flow beneath Arabia and East Africa, *Earth planet. Sci. Lett.,* **302,** 448–454.

Chang, S.-J., Merino, M., Van der Lee, S., Stein, S. & Stein, C., 2011. Mantle flow beneath Arabia offset from the opening Red Sea, *Geophys. Res. Lett.,* **38,** L04301, doi:10.1029/2010GL045852.

Christensen, N.I., 1996. Poisson's ratio and crustal seismology, *J. geophys. Res.,* **101,** 3139–3156.

Chu, D. & Gordon, R.G., 1998. Current plate motions across the Red Sea, *Geophys. J. Int.,* **135,** 313–328.

Courtillot, V., Jaupart, C., Manighetti, I., Tapponnier, P. & Besse, J., 1999. On causal links between flood basalts and continental breakup, *Earth planet. Sci. Lett.,* **166,** 177–195.

Cox, K.G., Gass, I.G. & Mallick, D.I.J., 1970. The peralkaline volcanic suites of Aden and Little Aden, South Arabia, *J. Petrol.,* **11,** 433–461.

d'Acremont, E., Leroy, S., Maia, M., Gente, P. & Autin, J., 2010. Volcanism, jump and propagation on the Sheba Ridge, eastern Gulf of Aden: segmentation evolution and implications for accretion processes, *Geophys. J. Int.,* **180,** 535–551.

Davison, I. *et al.*, 1994. Geological evolution of the southeastern Red Sea Rift margin, Republic of Yemen, *Geol. Soc. Am. Bull.,* **106,** 1474–1493.

Demets, C., Gordon, R.G. & Argus, D.F., 2010. Geologically current plate motions, *Geophys. J. Int.,* **181,** 1–80.

Direen, N.G., Stagg, H.M.J., Symonds, P.A. & Colwell, J.B., 2008. The architecture of volcanic rifted margins: new insights from the Exmouth-Gascoyne margin, Western Australia, *Aust. J. Earth Sci.,* **55,** 325–347.

Drake, C.L. & Girdler, R.W., 1964. A geophysical study of the Red Sea, *Geophys. J. R. astr. Soc.,* **8,** 473–495.

Dugda, M.T., Nyblade, A.A., Julia, J., Langston, C.A., Ammon, C.J. & Simiyu, S., 2005. Crustal structure in Ethiopia and Kenya from receiver function analysis: implications for rift development in eastern Africa, *J. geophys. Res.,* **110,** B01303, doi:10.1029/2004JB003065.

Eagles, G., Gloaguen, R. & Ebinger, C., 2002. Kinematics of the Danakil microplate, *Earth planet. Sci. Lett.,* **203,** 607–620.

Ebinger, C.J. & Casey, M., 2001. Continental breakup in magmatic provinces: an Ethiopian example, *Geology,* **29,** 527–530.

Efron, B. & Tibshirani, R., 1986. The Bootstrap Method for standard errors, confidence intervals, and other measures of statistical accuracy, *Stat. Sci.,* **1**(1), 1–35.

Egloff, F. *et al.*, 1991. Contrasting structural styles of the eastern and western margins of the southern Red Sea: the 1988 SONNE experiment, *Tectonophysics,* **198,** 329–353.

El-Anbaawy, M.I.H., Al-Aawah, M.A.H., Al-Thour, K.A. & Tucker, M., 1992. Miocene evaporites of the Red Sea Rift, Yemen Republic: sedimentology of the Salif halite, *Sedim. Geol.,* **81,** 61–71.

Fara, M., Chandrasekharam, D. & Minissale, A., 1999. Hydrogeochemistry of Damt thermal springs, *Yemen Republic, Geothermics,* **28,** 241–252.

Field, L., Barnie, T., Blundy, J., Brooker, R.A., Keir, D., Lewi, E. & Saunders, K., 2012. Integrated field, satellite and petrological observations of the November 2010 eruption of Erta Ale, *Bull. Volcanol.,* **74**(10), 2251–2271.

Fournier, M., Patriat, P. & Leroy, S., 2001. Reappraisal of the Arabia-India-Somalia triple junction kinematics, *Earth planet. Sci. Lett.,* **189,** 103–114.

Fournier, M. *et al.*, 2010. Arabia–Somalia plate kinematics, evolution of the Aden–Owen–Carlsberg triple junction, and opening of the Gulf of Aden, *J. geophys. Res.,* **115,** B04102, doi:10.1029/2008JB006257.

Frederiksen, A.W., Folsom, H. & Zandt, G., 2003. Neighbourhood inversion of teleseismic Ps conversions for anisotropy and layer dip, *Geophys. J. Int.,* **155,** 200–212.

Geoffroy, L., Huchon, P. & Khanbari, K., 1998. Did Yemeni tertiary granites intrude neck zones of a stretched continental upper crust? *Terra Nova,* **10,** 196–200.

Gernigon, L., Ringenbach, J.C., Planke, S. & Le Gall, B., 2004. Deep structures and breakup along volcanic rifted margins: insights from integrated studies along the outer Vøring Basin (Norway), *Mar. Petrol. Geol.,* **21**(3), 363–372.

Girdler, R.W., 1991. The case for ocean crust beneath the Red Sea, *Tectonophysics,* **198,** 275–278.

Girdler, R.W. & Styles, P., 1974. Two stage Red Sea floor spreading, *Nature,* **274,** 7–11.

Girdler, R.W. & Underwood, M., 1985. The evolution of early oceanic lithosphere in the southern Red Sea, *Tectonophysics,* **116,** 95–108.

Gladczenko, T., Hinz, K., Eldholm, O., Meyer, H., Neben, S. & Skogseid, J., 1997. South Atlantic volcanic margins, *J. geol. Soc.,* **154,** 465–470.

Gladczenko, T.P., Skogseid, J. & Eldholm, O., 1998. Namibia volcanic margin, *Mar. geophys. Res.,* **20,** 13–341.

Hammond, J.O.S., Kendall, J.M., Stuart, G.W., Keir, D., Ebinger, C.J., Ayele, A. & Belachew, M., 2011. The nature of the crust beneath the Afar triple junction: evidence from receiver functions, *Geochem. Geophys. Geosyst.,* **12,** doi:10.1029/2011GC003738.

Hansen, S.E., Rodgers, A.J., Schwartz, S.Y. & Al-Amri, A.M.S., 2007. Imaging ruptured lithosphere beneath the Red Sea and Arabian Peninsula, *Earth planet. Sci. Lett.,* **259,** 256–265.

Hébert, H., Deplus, C., Huchon, P., Khanbari, K. & Audin, L., 2001. Lithospheric structure of a nascent spreading ridge inferred from gravity data: the western Gulf of Aden, *J. geophys. Res.,* **106,** 26 345–26 363.

Hughes, G.W. & Beydoun, Z.R., 1992. The Red Sea–Gulf of Aden: biostratigraphy, lithostratigraphy and palaeoenvironments, *J. Petrol. Geol.,* **15,** 135–156.

International Seismological Centre, 2012. On-line Bulletin, http://www.isc.ac.uk, International Seismological Centre, Thatcham, United Kingdom.

Jestin, F., Huchon, P. & Gaulier, J.M., 1994. The Somalia plate and the East African Rift System: present kinematics, *Geophys. J. Int.,* **116,** 637–654.

Keen, C.E., Dickie, K. & Dehler, S.A., 2012. The volcanic margins of the northern Labrador Sea: insights to the rifting process, *Tectonics,* **31,** TC1011, doi:10.1029/2011TC002985.

Keir, D., Boatsow, I.D., Pagli, C. & Chambers, E.L., 2012. The development of extension and magmatism in the Red Sea rift of Afar, *Tectonophysics,* doi:10.1016/j.tecto.2012.10.015.

Kennett, B.L.N. & Engdahl, E.R., 1991. Traveltimes for global earthquake location and phase identification, *Geophys. J. Int.,* **122,** 429–465.

Kind, R. *et al.*, 2002. Seismic images of the crust and upper mantle beneath Tibet: evidence for Eurasian plate subduction, *Science,* **298,** 1219–1221.

Langston, C.A., 1977. Corvallis, Oregon, crustal and upper mantle structure from teleseismic P and S waves, *Bull. seism. Soc. Am.,* **67,** 713–724.

Langston, C.A., 1979. Structure under Mount Rainier, Washington, inferred from teleseismic body waves, *J. geophys. Res.,* **84,** 4749–4762.

Laughton, A.S. & Tramontini, C., l969. Recent studies of the crustal structure of the Gulf of Aden, *Tectonophysics,* **8,** 359–375.

Leroy, S. *et al.*, 2004. From rifting to spreading in the eastern Gulf of Aden: a geophysical survey of a young oceanic basin from margin to margin, *Terra Nova,* **16,** 185–192.

Leroy, S., d'Acremont, E., Tiberi, C., Basuyau, C., Autin, J. & Lucazeau, F., 2010a. Recent off-axis volcanism in the eastern Gulf of Aden: implications for plume-ridge interactions, *Earth planet. Sci. Lett.,* **293,** 140–153.

Leroy, S. *et al.*, 2010b. Contrasted styles of rifting in the eastern Gulf of Aden: a combined wide-angle MCS and Heat flow survey, *Geochem. Geophys. Geosyst.,* **11,** Q07004, doi:10.1029/2009GC002963.

Leroy, S. *et al.*, 2010c. Continental margins and Ocean-Continent Transitions of the Gulf of Aden: how Africa and Arabia broke up? Invited speaker. AGU Fall meeting San Francisco.

Leroy, S. *et al.*, 2012. From rifting to oceanic spreading in the Gulf of Aden: a synthesis, *Arab J. Geosci.,* **5**(5), 859–901.

Ligorria, J.P., 2000. An investigation of the crust-mantle transition beneath North America and the bulk composition of the North American crust, *PhD thesis,* Saint Louis University, p. 261.

Ligorria, J. & Ammon, G., 1999. Iterative deconvolution and receiver functions estimation, *Bull. seism. Soc. Am.,* **89,** 1395–1400.

Lucazeau, F. *et al.*, 2009. Post-rift volcanism and high heat-flow at the ocean–continent transition of the Gulf of Aden, *Terra Nova,* **21,** 285–292.

Makris, J., Henke, C.H., Egloff, F. & Akamaluk, T., 1991. The gravity field of the Red Sea and East Africa, *Tectonophysics,* **198,** 369–382.

McKenzie, D., 1978. Some remarks on the development of sedimentary basins, *Earth planet. Sci. Lett.,* **40,** 25–32.

McKenzie, D.P., Davies, D. & Molnar, P., 1970. Plate tectonics of the Red Sea and East Africa, *Nature,* **226,** 243–48.

Menzies, M.A., Klemperer, S.L., Ebinger, C.J. & Baker, J., 2002. Characteristics of volcanic rifted margins, in *Volcanic Rifted Margins: Geological Society of America Special Paper,* Vol. 362, pp. 1–14, eds Menzies, M.A., Klemperer, S.L., Ebinger, C.J. & Baker, J., Boulder, CO.

Milkereit, B. & Flüh, E.R., 1985. Saudi Arabian refraction profile: crustal structure of the Red Sea-Arabian shield transition, *Tectonophysics,* **111**(1985), 283–299.

Mjelde, R., Raum, T., Kandilarov, A., Murai, Y. & Takanami, T., 2009. Crustal structure and evolution of the outer Møre Margin, *NE Atlantic Tectonophys.,* **468,** 224–243.

Mohr, P., 1991. Structure of Yemeni dike swarms and emplacement of coeval granite plutons, *Tectonophysics,* **198,** 203–221.

Mooney, W.D., Gettings, M.E., Blank, H.R. & Healey, J.H., 1985. Saudi Arabian seismic refraction profile: a traveltime interpretation of crustal and upper mantle structure, *Tectonophysics,* **111,** 173–246.

Moseley, F., 1969. The Aden traps of Dhala, Musaymir and radfan, South Yemen, *Bull. Volcanol.,* **33,** 889–909.

Nobile, A., Pagli, C., Keir, D., Wright, T.J., Ayele, A., Joel, J. & Acocella, V., 2012. Dike-fault interaction during the 2004 Dallol intrusion at the northern edge of the Erta Ale Ridge (Afar, Ethiopia), *Geophys. Res. Lett.,* **39**(19), L19305, doi:10.1029/2012GL053152.

Owens, T.J., Zandt, G. & Taylor, S.R., 1984. Seismic evidence for an ancient rift beneath the Cumberland Plateau, Tennessee: a detailed analysis of broadband teleseismic P-waveforms, *J. geophys. Res.,* **89,** 7783–7795.

Prodehl, C., 1985. Interpretation of a seismic-refraction survey across the Arabian Shield in western Saudi Arabia, *Tectonophysics,* **111,** 247–282.

Prodehl, C. & Mechie, J., 1991. Crustal thinning in relationship to the evolution of the Afro-Arabian rift system: a review of seismic-refraction data, in *Red Sea: Birth and Early History of New Oceanic Basin,* eds Makris, J., Mohr, P. & Rihm, R., *Tectonophysics,* **198,** 311–327.

Rey, S.S., Planke, S., Symonds, P.A. & Faleide, J.I., 2008. Seismic volcanostratigraphy of the Gascoyne margin, western Australia, *J. Volcanol. Geotherm. Res.,* **172,** 112–131.

Ruegg, J.C., 1975. Main results about the crustal and upper mantle structure of the Djibouti region (T.F.A.I), in *Afar Depression of Ethiopia,* pp. 120–134, eds Pilger, A. & Rösler, A., Schweizerbart'sche Verlagsbuchhandlung, Stuttgart.

Sambridge, M., 1999a. Geophysical inversion with a neighbourhood algorithm-I. Searching a parameter space, *Geophys. J. Int.,* **138,** 479–494.

Sambridge, M., 1999b. Geophysical inversion with a neighbourhood algorithm-II. Appraising the ensemble, *Geophys. J. Int.,* **138,** 727–746.

Shibutani, T., Sambridge, M. & Kennett, B., 1996. Genetic algorithm inversion for receiver functions with application to crust and uppermost mantle structure beneath Eastern Australia, *Geophys. Res. Lett.,* **23**(14), doi:10.1029/96GL01671, issn:0094-8276.

Smith, L.K., White, R.S. & Kusznir, N.J., 2005. Structure of the Hatton Basin and adjacent continental margin, in *Petroleum Geology: North-West Europe and Global Perspectives. Proc 6th Petroleum Geology Conf,* pp. 947–956, eds Doré, A.G. & Vining, B.S., 6–9 October 2003, Geol. Soc.- London, London.

Stern, R.J. & Johnson, P., 2010. Continental lithosphere of the Arabian plate: a geologic, petrologic, and heophysical synthesis, *Earth Sci. Rev.,* **101,** 29–67.

Stuart, G.W., Bastow, I.D. & Ebinger, C.J., 2006. Crustal structure of the northern Main Ethiopian Rift from receiver function studies, in *The Afar Volcanic Province Within the East African Rift System,* Vol. 259, pp. 253–267, eds Yirgu, G., Ebinger, C.J. & Maguire, P.K.H., Geological Society, London, Special Publication.

Tard, F., Masse, P., Walgenwitz, F. & Gruneisen, P., 1991. The volcanic passive margin in the vicinity of Aden, Yemen. Bulletin Centres Recherche, *Exploration Prod. Elf-Aquitaine,* **15,** 1–9.

Tiberi, C., Ebinger, C., Ballu, V., Stuart, G. & Oluma, B., 2005. Inverse model of gravity data from the Red Sea-Aden-East African rifts triple junction zone, *Geophys. J. Int.,* **163,** doi:10.1111/j.1365-246X.2005.02736.

Tiberi, C., Leroy, S., d'Acremont, E., Bellahsen, N., Ebinger, C., Al-Lazki, A. & Pointu, A., 2007. Crustal geometry of the northeastern Gulf of Aden passive margin: localization of the deformation inferred from receiver function analysis, *Geophys. J. Int.,* **168,** 1247–1260.

Tramontini, C. & Davies, D., 1969. A seismic refraction survey in The Red Sea, *Geophys. J. R. astr. Soc.,* **17,** 225–241.

Ukstins, I.A., Renne, P.R., Wolfenden, E., Baker, J., Ayalew, D. & Menzies, M., 2002. Matching conjugate volcanic rifted margins: 40Ar/39Ar chrono-stratigraphy of pre- and syn-rift bimodal flood volcanism in Ethiopia and Yemen, *Earth planet. Sci. Lett.,* **198,** 289–306.

Watanabe, T., 1993. Effects of water and melt on seismic velocities and their application to characterization of seismic reflectors, *Geophys. Res. Lett.,* **20**(2), 933–936.

Watremez, L., Leroy, S., Rouzo, S., d'Acremont, E., Unternehr, P., Ebinger, C., Lucazeau, F. & Al Lazki, A., 2011. The crustal structure of the northeastern Gulf of Aden continental margin: insights from wide-angle seismic data, *Geophys. J. Int.,* **184,** 575–594.

White, R.S., Smith, L.K., Roberts, A.W., Christie, P.A.F., Kusznir, N.J. & Team, I., 2008. Lower crustal intrusion on the North Atlantic continental margin, *Nature,* **452**(7186), 460–464.

Wolfenden, E., Ebinger, C., Yirgu, G., Renne, P. & Kelley, S.P., 2005. Evolution of the southern Red Sea rift: birth of a magmatic margin, *Geol. Soc. Am. Bull.,* **117,** 846–864.

Zandt, G. & Ammon, C.J., 1995. Continental crust composition constrained by measurement of crustal Poisson's ratio, *Nature,* **374,** 152–154.

Zhu, L., 2000. Crustal structure across the San Andreas Fault, Southern California from teleseismic converted waves, *Earth planet. Sci. Lett.,* **179,** 183–190.

Zhu, L. & Kanamori, H., 2000. Moho depth variation in Southern California from teleseimic receiver function, *J. geophys. Res.,* **105,** 2969–2980.

SUPPORTING INFORMATION

Additional Supporting Information may be found in the online version of this article:

Figure S1. Receiver functions for 12 stations of the profile. The receiver functions are organized by increasing backazimuth (red number right of the trace). The light vertical lines indicate arrival times for conversion phases (Ps and multiples) from the Moho for the maximum stacking amplitude.

Figure S2. Thickness (*H*) versus *Vp/Vs* ratio diagrams from the *H-k* stacking method for the 12 stacked receiver functions shown in Fig. S1. The maximum of the stacking amplitude is indicated by the white point and corresponds to the value indicated in Table 1.

Figure S3. (Left) Seismic velocity models for MOKA station obtained from the neighbourhood algorithm method (Sambridge 1999a). The best 1000 models are indicated in yellow–green colour, and the best one (smallest misfit) corresponds to the red line, both for *S*-wave velocity and *Vp/Vs* ratio. (Right) Waveform matches between the observed individual (green) and stacked (blue) receiver functions and the predicted one (red) based on the best models (red lines in the left-hand diagrams). The white line in the left-hand diagram is the average velocity model.

Figure S4. (a) Left: Seismic velocity models for NE of ZUWA station obtained from the neighbourhood algorithm method (Sambridge 1999a). The best 1000 models are indicated in yellow–green colour, and the best one (smallest misfit) corresponds to the red line, both for *S*-wave velocity and *Vp/Vs* ratio. Right: waveform matches between the observed stacked receiver functions (blue) and the predicted one (red) based on the best models (red lines in the left-hand diagrams). The white line in the left-hand diagram is the average velocity model and light blue lines indicate the reference models of the velocity and *Vp/Vs* ratio. (b) Forward modelling of the ZUWA receiver function for backazimuth > 140°, signal displayed in black is the original RF and signal in red is the generated RF using the velocity model at the upper right corner.

Figure S5. An example of the inverted *H-k* values using different average crustal velocity *Vp* in the range 5.8–6.8 km s^{-1} is shown in (a). Solid lines are *Vp/Vs* as a function of crustal thickness *H* with bootstrap error estimates for the stacking method and dashed lines are from the initial velocity model for the NS section of the profile in (b), EW section of the profile in (c) and stations parallel to the Red Sea, south and east of plateau in (d). Three distinct error estimates were determined for the case of ZUWA station in (c), where the red ellipses represent the error estimate for the whole set of individual RF, green ellipses are error estimates for the receiver functions with backazimuth >140° (ZUWA S-W) and blue ellipses for the receiver functions with backazimuth <106° (ZUWA N-E). (http://gji.oxfordjournals.org/lookup/supp1/doi:10.1093/gji/ggt072/-/DC1).

Please note: Oxford University Press is not responsible for the content or functionality of any supporting materials supplied by the authors. Any queries (other than missing material) should be directed to the corresponding author for the article.